Title
Agricultural fires in the southeastern U.S. during SEAC4RS: Emissions of trace gases and particles and evolution of ozone, reactive nitrogen, and organic aerosol

Journal
Journal of Geophysical Research: Atmospheres, 121(12)

ISSN
2169-897X

Authors
Liu, Xiaoxi
Zhang, Y
Huey, LG
et al.

Publication Date
2016-06-27

DOI
10.1002/2016jd025040

AGU PUBLICATIONS

JGR

Journal of Geophysical Research: Atmospheres

RESEARCH ARTICLE
10.1002/2016JD025040

Special Section:
Studies of Emissions and Atmospheric Composition, Clouds and Climate Coupling by Regional Surveys, 2013 (SEAC4RS)

Agricultural fires in the southeastern U.S. during SEAC^{4}RS: Emissions of trace gases and particles and evolution of ozone, reactive nitrogen, and organic aerosol

Xiaoxi Liu[1], Y. Zhang[1], L. G. Huey[1], R. J. Yokelson[2], Y. Wang[1], J. L. Jimenez[3,4], P. Campuzano-Jost[3,4], A. J. Beyersdorf[5], D. R. Blake[6], Y. Choi[5,7], J. M. St. Clair[8,9,10], J. D. Crounse[8], D. A. Day[3,4], G. S. Diskin[5], A. Fried[11], S. R. Hall[12], T. F. Hanisco[9], L. E. King[1], S. Meinardi[6], T. Mikoviny[13], B. B. Palm[3,4], J. Peischl[4,14], A. E. Perring[4], I. B. Pollack[4,14], T. B. Ryerson[14], G. Sachse[5], J. P. Schwarz[14], I. J. Simpson[6], D. J. Tanner[1], K. L. Thornhill[5], K. Ullmann[12], R. J. Weber[1], P. O. Wennberg[8,15], A. Wisthaler[13,16], G. M. Wolfe[9,10], and L. D. Ziemba[5]

[1]School of Earth and Atmospheric Sciences, Georgia Institute of Technology, Atlanta, Georgia, USA, [2]Department of Chemistry, University of Montana, Missoula, Montana, USA, [3]Department of Chemistry and Biochemistry, University of Colorado Boulder, Boulder, Colorado, USA, [4]Cooperative Institute for Research in Environmental Sciences, University of Colorado Boulder, Boulder, Colorado, USA, [5]NASA Langley Research Center, Hampton, Virginia, USA, [6]Department of Chemistry, University of California, Irvine, California, USA, [7]Science Systems and Applications, Inc., Hampton, Virginia, USA, [8]Division of Geological and Planetary Sciences, California Institute of Technology, Pasadena, California, USA, [9]Atmospheric Chemistry and Dynamics Laboratory, NASA Goddard Space Flight Center, Greenbelt, Maryland, USA, [10]Joint Center for Earth Systems Technology, University of Maryland, Baltimore County, Catonsville, Maryland, USA, [11]Institute for Arctic and Alpine Research, University of Colorado Boulder, Boulder, Colorado, USA, [12]Atmospheric Chemistry Observations and Modeling Laboratory, National Center for Atmospheric Research, Boulder, Colorado, USA, [13]Department of Chemistry, University of Oslo, Oslo, Norway, [14]Earth System Research Laboratory, National Oceanic and Atmospheric Administration, Boulder, Colorado, USA, [15]Division of Engineering and Applied Science, California Institute of Technology, Pasadena, California, USA, [16]Institute of Ion Physics and Applied Physics, University of Innsbruck, Innsbruck, Austria

Key Points:
- Emission factors measured for 15 agricultural fires in the southeastern U.S.
- Ozone, PAN, and nitrate formed in aged plumes, and O/C of OA increased
- Chemical evolution simulated by a Lagrangian plume cross-section model

Supporting Information:
- Supporting Information S1

Correspondence to:
L. G. Huey,
greg.huey@eas.gatech.edu

Citation:
Liu, X., et al. (2016), Agricultural fires in the southeastern U.S. during SEAC^{4}RS: Emissions of trace gases and particles and evolution of ozone, reactive nitrogen, and organic aerosol, *J. Geophys. Res. Atmos.*, *121*, 7383–7414, doi:10.1002/2016JD025040.

Received 4 MAR 2016
Accepted 25 MAY 2016
Accepted article online 28 MAY 2016
Published online 22 JUN 2016

Abstract Emissions from 15 agricultural fires in the southeastern U.S. were measured from the NASA DC-8 research aircraft during the summer 2013 Studies of Emissions and Atmospheric Composition, Clouds and Climate Coupling by Regional Surveys (SEAC^{4}RS) campaign. This study reports a detailed set of emission factors (EFs) for 25 trace gases and 6 fine particle species. The chemical evolution of the primary emissions in seven plumes was examined in detail for ~1.2 h. A Lagrangian plume cross-section model was used to simulate the evolution of ozone (O_3), reactive nitrogen species, and organic aerosol (OA). Observed EFs are generally consistent with previous measurements of crop residue burning, but the fires studied here emitted high amounts of SO_2 and fine particles, especially primary OA and chloride. Filter-based measurements of aerosol light absorption implied that brown carbon (BrC) was ubiquitous in the plumes. In aged plumes, rapid production of O_3, peroxyacetyl nitrate (PAN), and nitrate was observed with $\Delta O_3/\Delta CO$, $\Delta PAN/\Delta NO_y$, and $\Delta nitrate/\Delta NO_y$ reaching ~0.1, ~0.3, and ~0.3. For five selected cases, the model reasonably simulated O_3 formation but underestimated PAN formation. No significant evolution of OA mass or BrC absorption was observed. However, a consistent increase in oxygen-to-carbon (O/C) ratios of OA indicated that OA oxidation in the agricultural fire plumes was much faster than in urban and forest fire plumes. Finally, total annual SO_2, NO_x, and CO emissions from agricultural fires in Arkansas, Louisiana, Mississippi, and Missouri were estimated (within a factor of ~2) to be equivalent to ~2% SO_2 from coal combustion and ~1% NO_x and ~9% CO from mobile sources.

1. Introduction

Biomass burning (BB) produces significant amounts of trace gases and aerosol, which play important roles in atmospheric chemistry and climate [*Crutzen and Andreae*, 1990]. One important component of BB is agricultural field burning, a common practice worldwide. Emissions of global agricultural residue burning have been estimated as the fourth largest among all types of BB [*Andreae and Merlet*, 2001]. An estimated 500 Tg of crop residues was burned in fields annually in the developing world in the 1990s [*Yevich and Logan*, 2003]. Agricultural field burning is also extensive in the contiguous United States [*McCarty*, 2011], where wheat, rice,

sugarcane, peanut, soybeans, barley, and corn croplands are thought to have the most significant burning activity [*Dennis et al*., 2002].

Agricultural fire emissions can have a large impact on atmospheric composition and air quality on regional scales. Previous studies demonstrated that the open burning of crop residues is a significant source of trace gases and aerosols such as carbon dioxide (CO_2), carbon monoxide (CO), methane (CH_4), nonmethane hydrocarbons, nitrogen oxides (NO_x), ammonia (NH_3), sulfur dioxide (SO_2), black carbon (BC), organic aerosol (OA), and inorganic particulate matter [*Dennis et al*., 2002; *McCarty*, 2011; *Huang et al*., 2012; *Kudo et al*., 2014]. These emissions can lead to severe air quality problems. For example, *Zhang et al*. [2015] found that primary emissions from BB, mainly crop residue burning, contributed to 25 ± 8% of elemental carbon (EC) and 40–65% of nonfossil organic carbon (OC) in four major cities in China during an extreme haze episode in winter 2013. Despite the important impacts of the emissions from agricultural burning, emission inventories are not well characterized. The uncertainty in agricultural burning emissions is primarily due to two factors: (1) many of the emitted species are rarely measured or even identified; and (2) the burn area and/or the fraction of crop residue burned are highly uncertain [*McCarty et al*., 2009; *Randerson et al*., 2012].

Field measurements from airborne and ground-based platforms are able to sample plumes in the complex, natural environment and are a valuable method to characterize fire emissions and evolution. However, field measurements of agricultural burning are scarce and have been mainly conducted in Mexico and China [*Yokelson et al*., 2009, 2011; *Kudo et al*., 2014]. Laboratory studies are also an important method to characterize BB smoke. Recently, the fourth Fire Lab at Missoula Experiment (FLAME-4) conducted laboratory burning studies of trace gas and particle emissions and their subsequent evolution from several types of crop residues collected from various countries [*Stockwell et al*., 2014]. These lab-burned crop residues include fuels that are important in the U.S., such as sugarcane, rice straw, and wheat straw.

The area of agricultural burning is usually estimated by surveys, conducted by state agencies, or by remote sensing [*McCarty et al*., 2009; *Melvin*, 2012; *Randerson et al*., 2012]. Both methods can underestimate the area burned and thus the magnitude of emissions. The survey method is limited as few states collect agricultural burning information and burning practices vary widely from state to state. Remote sensing methods have difficulty with detecting agricultural fires as they are often short lived and relatively small [*Smith et al*., 2007; *Hawbaker et al*., 2008; *Chang and Song*, 2010; *van der Werf et al*., 2010].

Chemical and physical transformations of primary fire emissions can lead to significant changes in the gaseous and particulate phase composition of the smoke [*Hobbs et al*., 2003; *Jost et al*., 2003; *Yokelson et al*., 2009; *Akagi et al*., 2012]. Therefore, understanding smoke evolution is an important issue. The chemical evolution of trace gases can influence the formation of ozone (O_3) and the conversion of NO_x to other reactive nitrogen (NO_y) species such as peroxyacetyl nitrate (PAN) and particulate nitrate. O_3 enhancement is common in tropical BB plumes, while both O_3 production and destruction have been observed in boreal BB plumes [*Goode et al*., 2000; *Hobbs et al*., 2003; *Yokelson et al*., 2009; *Alvarado et al*., 2010; *Singh et al*., 2010; *Jaffe and Wigder*, 2012]. In temperate regions, the few available field studies of BB sampled prescribed fires and observed O_3 enhancement [*Trentmann and Andreae*, 2003; *Akagi et al*., 2012, 2013; *Müller et al*., 2016]. *Jaffe and Wigder* [2012] reviewed numerous factors that influence O_3 production from wildfires, including emissions of O_3 precursors such as NO_x and nonmethane organic compounds (NMOCs), combustion efficiency, photochemistry, aerosol effects on chemistry and radiation, and local and downwind meteorological patterns. PAN formation in the first few hours after emission has been observed in plumes of several types of BB, such as a chaparral fire in California, a small forest fire in Georgia, and boreal forest fires [*Yokelson et al*., 2009; *Alvarado et al*., 2010; *Akagi et al*., 2012; *Müller et al*., 2016]. The transport of PAN potentially influences O_3 formation downwind [*Jacob et al*., 1992; *Leung et al*., 2007; *Jaffe and Wigder*, 2012]. However, there are still questions regarding PAN photochemistry since some previous modeling studies were not able to successfully simulate the observed concentrations of O_3 and PAN in different BB plumes [*Trentmann et al*., 2005; *Alvarado and Prinn*, 2009]. One exception is a recent study by *Müller et al*. [2016], which accurately modeled O_3 and PAN formation during the first hour of aging for a small forest fire in Georgia using the observations of 16 nonmethane organic gases, CH_4, NO_x, nitrous acid (HONO), CO, and O_3. Another important plume process is the formation of secondary organic aerosol (SOA). Highly variable SOA formation rates in aging BB smoke have been reported, although limited net increase in OA mass is often observed [*Capes et al*., 2008; *Yokelson et al*., 2009; *Cubison et al*., 2011; *Hecobian et al*., 2011; *Jolleys et al*., 2012; *Vakkari et al*., 2014]. Brown carbon

(BrC), a component of OA that absorbs light in the UV and visible spectral regions, is associated with incomplete combustion and SOA formation [*Hecobian et al*., 2011; *Saleh et al*., 2013; *Forrister et al*., 2015]. Recent studies indicate that BrC evolution in BB plumes is controlled by secondary processes such as chromophore formation and loss due to photobleaching, volatilization, and/or aerosol phase reactions, leading to different evolution of BrC and bulk OA [*Lee et al*., 2014; *Zhong and Jang*, 2014; *Forrister et al*., 2015; *Zhao et al*., 2015]. Although agricultural field burning is ubiquitous in the U.S., no field study to date has characterized the emissions and smoke chemistry of these fires.

A major goal of the recent Studies of Emissions and Atmospheric Composition, Clouds, and Climate Coupling by Regional Surveys (SEAC^{4}RS) airborne field campaign was to quantify the emissions and assess the atmospheric impacts of agricultural and forest fires. The heavily instrumented NASA DC-8 research aircraft was deployed during this mission, which enabled measurements of a wide variety of chemical species and physical parameters [*Toon et al*., 2016]. During SEAC^{4}RS, five research flights targeted agricultural fire plumes during late summer of 2013.

This study presents the first detailed measurements of trace gas and fine particle emissions from 15 agricultural fires in the U.S., with locations shown in Figure 1. The vegetation burned is almost certainly rice straw because it is essentially the only crop residue burned in the Mississippi River Valley during the late summer and early fall [*McCarty et al*., 2007]. The evolution of O_3 and reactive nitrogen species (PAN, NO_x, HNO_3, and nitrate) in these fire plumes is examined in detail. The changes of OA concentration and BrC absorption in the first 1.2 h of aging are also investigated. To evaluate our understanding of the rapid chemical evolution within fire plumes in a biogenically influenced environment, a Lagrangian plume cross-section (LPCS) model is used to simulate the formation of O_3, PAN, and nitrate. By implementing the simple parameterization proposed by *Hodzic and Jimenez* [2011], the model also simulates SOA and the change of atomic oxygen-to-carbon (O/C) ratios that characterize OA oxidation state. With the measured emission factors (EFs), we also estimate the annual agricultural fire emissions of SO_2, NO_x, and CO from the four states where the fires were sampled.

2. Methods

2.1. Aircraft Instrumentation

A wide range of chemical, physical, and optical measurements were used to characterize the agricultural fires. These measurements are listed in Table 1 along with methodologies, sample intervals, accuracies, and references. All the data used in this work can be accessed through the NASA data archive (http://www-air.larc.nasa.gov/cgi-bin/ArcView/seac4rs, doi: 10.5067/Aircraft/SEAC4RS/Aerosol-TraceGas-Cloud). All data used were synchronized to match the rapid measurements of ambient water vapor, which ensured accurate peak alignment.

2.2. Airborne Sampling of Fires

The aircraft sampled agricultural fires during the five research flights by either cross-plume or long-axis penetrations at its typical air speeds in the range ~110–150 m s^{-1}. Figure S1 in the supporting information includes two photographs taken from NASA DC-8 cameras showing two typical fires and the emanating plumes that were sampled. Figure S2 exemplifies two time series obtained following each strategy. The cross-plume transects were usually performed at or near the source at altitudes ranging from 0.3 to 1.3 km above the ground, which provided observations of fresh smoke younger than several minutes. However, since such sampling requires high time resolution measurements, some instruments could not get sufficient data, especially for small fires. Therefore, the long-axis sampling strategy, including source-to-downwind and downwind-to-source approaches, was also performed for some agricultural fires. The aircraft conducted the long-axis source-to-downwind sampling by entering the smoke column very close to the active flame front at an altitude between 0.2 and 1.3 km, mostly below 0.5 km. Maximum performance climbs were then attempted to match the rise of the smoke and to extend sampling in the smoke. As the plane flew down the long axis, it entered or exited both thicker and thinner plume regions, creating a series of peaks due to intermittent sampling of higher concentrations along the plume length. The sample age for each peak was calculated by dividing the downwind distance from the source by average wind speed, calculated using 3-D wind measurements [*Chan et al*., 1998]. The source locations usually preceded the largest fresh peak by a few hundred meters since the smoke rose at an angle. The downwind-to-source sampling was performed as the reverse of the source-to-downwind sampling. With the long-axis strategy, the aircraft

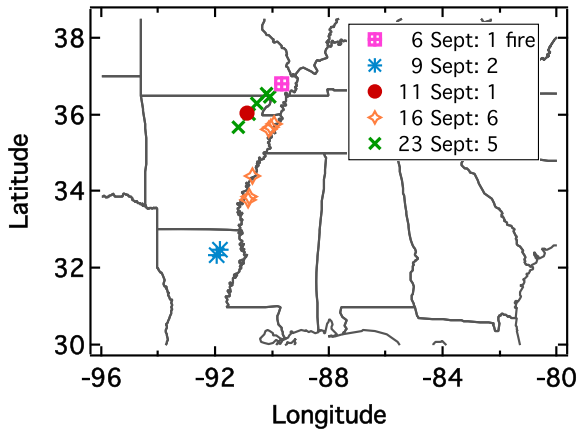

Figure 1. Locations of the 15 agricultural fires during the SEAC^{4}RS campaign.

acquired samples of both fresh and aged plumes up to ~16 km downwind and ~1.2 h old. Figure 2 shows an example of a partial flight path over Arkansas on 23 September 2013 along with the locations of the five agricultural fires sampled. Table 2 summarizes the sampling times and locations of the 15 agricultural fires and the number of samples obtained by each of the two sampling strategies. Of the 15 fires, the sources of 12 fires were recorded by the aircraft cameras. The locations of these fires are defined as the centers of the burning fields with an accuracy of ~300 m for a typical sized field. For the three fires for which sources were not recorded, their source locations were defined as the point where the 1 s CO concentration was highest in each plume sample. The locations of the 15 fires are also displayed in Figure 1.

2.3. Estimation of Emission Ratios, Emission Factors, and Modified Combustion Efficiency

The enhancements of CO and CO_2 (the two main gaseous emissions from BB) were examined for all five flights to identify and delineate the edges of all agricultural burning plumes. BB tracers such as hydrogen cyanide (HCN) and acetonitrile (CH_3CN) were then used to confirm that the CO and CO_2 enhancements were due

Table 1. Aircraft Measurements Aboard the NASA DC-8 Research Aircraft During SEAC^{4}RS

Measurement	Method	Sample Interval	Calibration Accuracy	Reference
SO_2 and HCl	SF_6^- chemical ionization mass spectrometry (CIMS)	0.5 s and 0.1 s at 1.2 s[a]	15–25%	*Huey et al.* [2004]
PAN	I^- CIMS	0.5 s at 2 s[a]	15%	*Slusher et al.* [2004]
NO, NO_2, NO_y, and O_3	Chemiluminescence	1 s	3–15%	*Ryerson et al.* [1999] and *Ryerson et al.* [2000]
VOCs and OVOCs[b]	Proton transfer reaction mass spectrometry	0.1 s at 10 s[a]	5–15%	*Wisthaler et al.* [2002]
NMHCs	Whole air sampling and gas chromatography	30–60 s	1–5%	*Blake et al.* [2003] and *Simpson et al.* [2011]
CO	Differential absorption CO measurement	1 s	5%	*Sachse et al.* [1987] and *Diskin et al.* [2002]
CO_2	Nondispersive infrared spectrometer	1 s	0.25 ppm	*Vay et al.* [2011]
HNO_3, HCN, H_2O_2, hydroxyacetone, HPALDs, isoprene hydroxynitrates, and MVK/MACR nitrates	CF_3O^- CIMS	1 s	30–50%	*Crounse et al.* [2006], *St. Clair et al.* [2014], and *Paulot et al.* [2009a]
Formaldehyde	Laser-induced fluorescence[c]/difference frequency generation absorption spectroscopy[d]	1 s	4–10%	*Cazorla et al.* [2015], *Weibring et al.* [2006], and *Weibring et al.* [2007]
Nonrefractory submicron aerosol (sulfate, nitrate, ammonium, chloride, and organics)[e]	High-resolution time-of-flight mass spectrometry	1 s	34–38%	*Canagaratna et al.* [2007] and *Canagaratna et al.* [2015]
Black carbon aerosol[f]	Laser-induced incandescence	1 s	30%	*Schwarz et al.* [2013]
Particle absorption coefficients	Radiance research particle soot absorption photometer	1 s	5%	*Virkkula et al.* [2005]
Photolysis frequencies	Spectral radiometry	3 s	~12–25%	*Shetter and Müller* [1999]

[a]Disjunct sampling.
[b]In the case of multiple neutral precursors for a specific *m/z* signal, we consider only species with a relative contribution > 10% to the total signal [*Yokelson et al.*, 2013; *Stockwell et al.*, 2015; *Müller et al.*, 2016].
[c]Used to derive CH_2O emissions for the flights on 6, 9, 11, and 16 September 2013.
[d]Used to derive CH_2O emissions for the flight on 23 September 2013 when laser-induced fluorescence measurement was not available.
[e]Particle diameter less than 1 μm.
[f]Particle diameter range is ~90–550 nm.

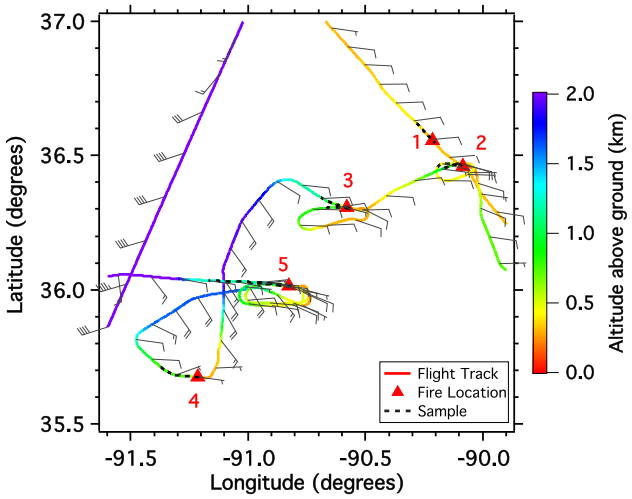

Figure 2. Fires sampled and DC-8 flight track with wind barbs on 23 September 2013. Flight track is colored by aircraft radar altitude. Red triangles represent the locations of the five agricultural fires sampled. Dashed black lines represent plume samples obtained.

to BB. For all the identified plumes, the following quantities were derived: excess mixing ratio, normalized excess mixing ratio (NEMR), emission ratio (ER), emission factor (EF), and modified combustion efficiency (MCE). These parameters were then used to characterize initial emissions and plume evolution. The excess mixing ratio of a species X (ΔX) was calculated by subtracting the mixing ratio of X in the background air from that in the fire plume. The background concentrations were based on measurements made ~30 s before or after the plume encounter, at a similar location and altitude as the sampled plume. For this time period, both continuous and discrete instruments acquired sufficient data in background air. The NEMR was derived by dividing ΔX by the excess mixing ratio of a simultaneously measured species Y, where Y was usually a relatively long-lived tracer such as CO or CO_2 that enabled the NEMR to account for the influence of dilution. A special case of the NEMR is the emission ratio (ER), which is $\Delta X/\Delta Y$ specifically in fresh smoke up to a few minutes old sampled at or near the fire source. As shown in Table 1, the data used in this study were generated from various continuous and discrete instruments with different time resolutions and response times. To allow comparison between different instruments, NEMRs (or ERs) were obtained by comparing the integrals of ΔX and ΔY of a series of peaks as the aircraft passed through an aged (or nascent) smoke plume (SO_2 and BC are shown as examples in Figure 3).

The ER has two important uses: (1) it can be used to calculate EFs, and (2) differences between the ERs measured at the source and the NEMRs measured downwind allow us to quantify gas and particulate phase chemistry and gas-particle partitioning. Fire-averaged ERs were used to compute EFs. The fire-averaged molar ERs for gaseous species and mass ERs for particulate species relative to CO_2 or CO for each individual fire were computed as follows. First, if only one fresh plume transect was available for a fire, the ER for this fire was the ratio between

Table 2. Details of the Agricultural Fires Sampled in the Southeastern U.S.

Date	Fire #	Local Time	Latitude	Longitude	Field Size[a] (ha)	Location	No. of Cross-Plume Samples	No. of Long-Axis Samples
6 Sep	1[b]	13:57–13:58	36.8143	−89.6778	22.27	Missouri	0	1
			36.8217	−89.6752	43.61			
9 Sep	2[c]	18:22	32.4714	−91.8541	-	Louisiana	1	0
	3	18:35–19:19	32.3365	−91.9755	37.24	Louisiana	2	4
11 Sep	4	14:53–15:01	36.0497	−90.8913	127.59	Arkansas	0	2
16 Sep	5	17:21–17:25	35.7742	−89.9388	30.39	Arkansas	0	2
	6[c]	17:27	35.6636	−90.0629	-	Arkansas	0	1
	7	17:32–17:33	35.6278	−90.1471	26.94	Arkansas	0	2
	8	17:49–17:50	34.4073	−90.7022	22.58	Arkansas	0	1
	9	17:57	33.8702	−90.8243	17.15	Mississippi	0	1
	10	17:58–17:59	33.7876	−90.8746	21.64	Mississippi	0	1
23 Sep	11[c]	13:43–13:44	36.5622	−90.2199	-	Missouri	1	0
	12	13:46–14:05	36.4647	−90.0898	30.97	Missouri	1	2
	13	14:09–14:21	36.3024	−90.5659	27.62	Arkansas	1	2
	14	14:31–14:33	35.6727	−91.2077	18.15	Arkansas	0	1
	15	14:46–15:07	36.0128	−90.8144	16.35	Arkansas	0	3

[a]Determined using Google Earth.
[b]Two adjacent fields were burning at the same time, and their plume columns merged into a single plume.
[c]Fires for which the sources were not recorded by the aircraft cameras.

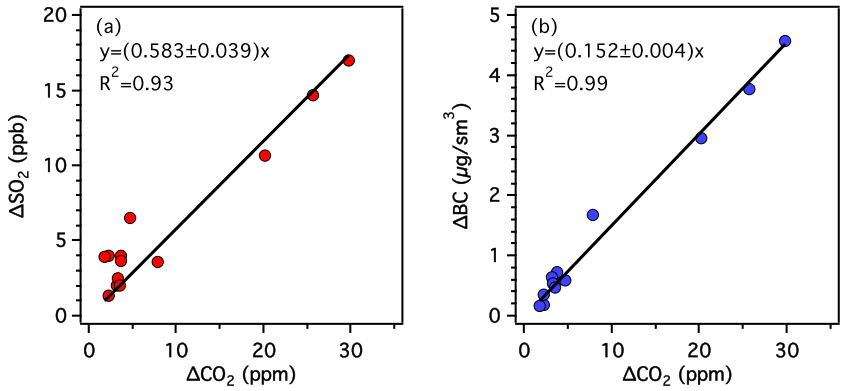

Figure 3. Emission ratio plots of (a) $\Delta SO_2/\Delta CO_2$ and (b) $\Delta BC/\Delta CO_2$ from Fire 4 on 11 September 2013.

the integral of ΔX over the entire fresh plume relative to that of ΔCO_2 or ΔCO over the entire fresh plume. Second, for multiple discrete samples of a fire, the fire-averaged ER was obtained from the slope of the least squares line (with the intercept forced to zero) in a plot of one set of integrals of excess mixing ratios versus another [*Yokelson et al.*, 2009]. However, species measured by the PTR-MS were treated differently, because they were reported for 0.5–1 s measurements at a lower time resolution of every ~10 s. Potential errors due to different sampling frequencies limit deriving the ERs of these species directly from ΔX/ΔCO in an environment with rapidly changing concentrations. For these species, we first obtained the ER relative to PTR-MS benzene averaged over each fire by comparing the integrated excess for an entire fire to the integrated excess amount for benzene. As benzene was also measured by the whole air sampling (WAS) system at time resolutions of 30–60 s, this facilitated obtaining ERs of PTR-MS species relative to ΔCO. To be specific, these ERs can be obtained by multiplying the ER of Δ(PTR-MS species)/Δ(PTR-MS benzene) by the fire-averaged ER of Δ(WAS benzene)/ΔCO, with Δ(WAS benzene) and ΔCO integrated over the same period within the plume. For the three fires where WAS benzene was not available (Fires 2, 7, and 11), the fire-averaged ERs of Δ(PTR-MS benzene)/ΔCO were used for obtaining ERs of PTR-MS species, in which Δ(PTR-MS benzene) and ΔCO were averaged over the same sampling time.

Emissions undergo chemical and physical changes that can deplete or enhance their mixing ratios. In this study, short-lived compounds are defined as those with lifetimes less than ~1 day [*Atkinson and Arey*, 2003; *Atkinson et al.*, 2006; *Simpson et al.*, 2011]. To further identify any other reactive compounds, the NEMR of each species, which was obtained from long-axis samples, was plotted versus smoke age to identify possible evolution. For both the short-lived compounds and the longer-lived compounds that also exhibited evolution, the fire-averaged ERs were calculated only using the fresh samples that were less than ~10 min old and sampled within ~3 km of the sources where CO concentrations peaked. These reactive compounds include nitrogen monoxide (NO), nitrogen dioxide (NO_2), formaldehyde, acetaldehyde, isoprene/furan plus isomeric pentadienes and cyclopentene, monoterpenes, methyl vinyl ketone (MVK) plus its isomers methacrolein (MACR) and crotonaldehyde, nitrate, ammonium, and OA. The long-axis sampling strategy often gave interinstrument NEMRs at a series of typically 5–10 downwind ages up to ~1.2 h, which also enabled characterizing downwind plume evolution of reactive compounds. However, besides plume evolution, the changes occurring downwind can also reflect changes at the source that occurred before the aircraft arrived. In most cases the source changes can be assumed to be small as the fire burned through a homogeneous fuel bed in a single crop type. The cases where source combustion regime changes were contributing can be identified by looking at the ΔBC/ΔCO ratio as a surrogate for the flaming to smoldering ratio [*Yokelson et al.*, 2009]. For all except one fire (Fire 12) in which BC was measured, the average ΔBC/ΔCO ratios for the last few ages were similar to the ΔBC/ΔCO ratios near the sources within measurement uncertainty (Figure S3). In addition, there was generally no apparent relationship between the observed small ΔBC/ΔCO variations and the evolution of O_3, PAN, or OA (r^2 of ΔBC/ΔCO versus $\Delta O_3/\Delta CO$ or ΔPAN/ΔCO ranged from 0.001 to 0.37). The exceptions are the relatively good correlations between ΔBC/ΔCO and $\Delta O_3/\Delta CO$ ($r^2 = 0.61$) and ΔPAN/ΔCO ($r^2 = 0.86$) for Fire 12 and that between ΔBC/ΔCO and ΔOA/ΔCO ($r^2 = 0.77$) for Fire 13. Except for these cases, we concluded that the downwind changes described here were driven mainly by chemical and physical evolution rather than source changes with time.

EFs, in units of grams of compound X emitted per kilogram of dry biomass burned, were derived for all the individual fires using the carbon mass balance method, which assumes that all the volatilized carbon is detected [*Yokelson et al*., 1999]:

$$EF_X = F_C \times MW_X / MW_C \times C_X / C_T \quad (1)$$

where F_C is the carbon mass fraction for which we use a value of 39.3 ± 2.4%, which is an average of rice straw collected from California and Arkansas, U.S. and from China based on elemental analysis (ALS Analytics, Tucson); MW_X and MW_C are the molecular weight of compound X and the atomic weight of carbon, respectively; and C_X/C_T is the number of emitted moles of compound X divided by the total number of moles of carbon emitted. C_X/C_T was calculated using

$$\frac{C_X}{C_T} = \frac{\frac{\Delta C_X}{\Delta CO_2}}{\sum_{j=1}^{n}\left(nC_j \times \frac{\Delta C_j}{\Delta CO_2}\right)} \quad (2)$$

where $\Delta C_X/\Delta CO_2$ and $\Delta C_j/\Delta CO_2$ are the fire-averaged ER of species X to CO_2 and that of carbon-containing species j to CO_2, respectively; and nC_j is the number of carbon atoms in compound j. The sum of the moles of carbon divided by the emitted moles of CO_2, the denominator in equation (2), was determined from the measured carbon-containing species including CO_2 and CO. Sources of uncertainties that contribute to the overall uncertainty of individual EFs include (in order of significance): (1) the uncertainties in the integrated ΔX vary by species and fire, but are usually near instrumental uncertainties (Table 1) given the significant enhancements in fresh plumes; (2) the uncertainties in the slopes of ΔX versus ΔY are usually small (<5%) while the ER-derivation method for PTR-MS species is likely associated with another ~20% uncertainty; (3) the ~6% uncertainty in the carbon mass fraction; and (4) the sum of the moles of carbon determined from CO_2 and CO could underestimate the total carbon by 2–4%, which would lead to an overestimation of EFs by 2–4% [*Akagi et al*., 2011]. In contrast to the individual EF uncertainty, fire-to-fire variability is the dominant uncertainty (≥40% except for CO_2 and CO) and is reported throughout.

BB emissions also vary with different combustion processes, e.g., flaming and smoldering. The MCE, which describes the relative amount of flaming or smoldering [*Akagi et al*., 2011], was also calculated. MCE is defined as $\Delta CO_2/(\Delta CO_2 + \Delta CO)$. Higher MCE values indicate more flaming combustion and lower MCE more smoldering combustion. Pure flaming has an MCE near 0.99, while smoldering has an MCE over a larger range (~0.65–0.85) but is most often near 0.8. An overall fire-integrated MCE near 0.9 suggests roughly equal amounts of flaming and smoldering [*Akagi et al*., 2011]. Fire-integrated MCEs are presented here for comparison to fire-averaged EFs.

2.4. Calculation of BrC Absorption

Particle absorption coefficients measured at two wavelengths (470 and 532 nm) by a particle soot absorption photometer (PSAP) were used to infer BrC absorption in fire plumes [*Lack and Langridge*, 2013]. PSAP data were corrected for a known scattering interference from particles deposited on the collection media based on *Virkkula* [2010]. The aerosol absorption Ångström exponent (AAE) was determined from a pair of observations at 470 and 532 nm and then used to estimate the aerosol absorption at 365 and 660 nm, using equations (3)–(5).

$$AAE_{PSAP} = -\frac{ln\left(b_{ap,PSAP}(532)\right) - ln\left(b_{ap,PSAP}(470)\right)}{ln(532) - ln(470)} \quad (3)$$

$$b_{ap,PSAP}(365) = b_{ap,PSAP}(532)\left(\frac{365}{532}\right)^{-AAE_{PSAP}} \quad (4)$$

$$b_{ap,PSAP}(660) = b_{ap,PSAP}(470)\left(\frac{660}{470}\right)^{-AAE_{PSAP}} \quad (5)$$

The light absorption by BC at 365 nm ($b_{ap,BC}(365)$) can then be derived by extrapolation using $b_{ap,PSAP}(660)$ and a BC AAE of 1 [*Bergstrom et al*., 2002; *Kirchstetter et al*., 2004; *Schnaiter et al*., 2005], assuming that absorption at 660 nm is mainly due to BC and that the BrC contribution is minimal [*Liu et al*., 2014].

$$b_{ap,BC}(365) = b_{ap,PSAP}(660)\left(\frac{365}{660}\right)^{-AAE_{BC}} \quad (6)$$

BrC absorption at 365 nm ($b_{ap,BrC}(365)$) was then determined as the difference between $b_{ap,PSAP}(365)$ and $b_{ap,BC}(365)$. For each fire, we calculated fresh ER and downwind NEMRs of $\Delta b_{ap,BrC}(365)/\Delta CO$, $\Delta b_{ap,BC}(365)/\Delta CO$, and $\Delta b_{ap,PSAP}(365)/\Delta CO$.

Using PSAP data to predict BrC absorption is an indirect method that has inherent uncertainties. AAE_{PSAP}, given in equation (3), can be determined from different wavelength combinations (i.e., 470–532, 470–660, and 532–660 nm). For SEAC[4]RS data set, only one wavelength pair 470–532 nm is available. Measurement uncertainty of PSAP (5%) results in a 7% uncertainty in AAE_{PSAP}. *Liu et al*. [2015] and *Liu et al*. [2014] found that different pairs led to systematically different $b_{ap,PSAP}(365)$, predicted by equations (3) and (4). They found that the 470–660 nm pair gave results for $b_{ap,PSAP}(365)$ in between the other pairs. The 470–532 nm pair and the 532–660 nm pair resulted in $b_{ap,PSAP}(365)$ that was ~20% higher and ~20% lower than the 470–660 nm pair, respectively. Thus, our $b_{ap,PSAP}(365)$ estimated from the 470-532 nm pair likely has an uncertainty of 17%, when compared to the middle $b_{ap,PSAP}(365)$ predicted from the 470–660 nm pair. Another uncertainty comes from the attribution of BC. For example, since BC internally mixed with nonabsorbing material would have an AAE_{BC} greater than 1, the attributed short-wavelength BC absorption was likely underestimated [*Lack and Langridge*, 2013]. *Lack and Langridge* [2013] proposed that the uncertainty in short-wavelength (404 nm) absorption by BC determined by extrapolation using an $AAE_{BC} = 1$ ranged from +7% to −22%. For this reason, we used 22% as an approximate uncertainty for the predicted $b_{ap,BC}(365)$. The uncertainties of the AAE attribution method and the PSAP measurement (5%) were then treated independently and propagated in quadrature yielding uncertainties in $b_{ap,PSAP}(365)$ and $b_{ap,BC}(365)$ of 19% and 23%, respectively. By combining these two uncertainties, the uncertainty in $b_{ap,BrC}(365)$ is estimated to be 20%–43%. Due to uncertainties associated with these various calculations, definitively attributing the difference to be due to BrC is highly uncertain. However, for BB plumes sampled in an airborne study, *Liu et al*. [2015] derived a reasonable closure (a slope within 22% of 1) between BC + filter-based BrC versus absorption coefficients derived from the PSAP wavelength pair 470–660 nm, which suggests that PSAP AAEs greater than 1 were mainly due to the presence of BrC. Analogous to individual EFs, individual $\Delta b_{ap,BrC}(365)/\Delta CO$ in fresh plumes likely have an uncertainty of 21%–43% by combining the uncertainties in $b_{ap,BrC}(365)$ and CO measurements. The accuracy of downwind $\Delta b_{ap,BrC}(365)/\Delta CO$ may be slightly reduced by the diluted concentrations.

2.5. Lagrangian Plume Cross-Section Model

We developed a Lagrangian plume cross-section (LPCS) model based on the 1-D version of the Regional chEmical trAnsport Model (1-D REAM) [*Wang et al*., 2007; *Gray et al*., 2010; *Liu et al*., 2010, 2012; *Zhang et al*., 2014, 2016]. This LPCS-REAM model was used to simulate the evolution of agricultural fire emissions. Differing from previous modeling approach that treated the plume as a well-mixed Lagrangian parcel [*Mason et al*., 2006; *Alvarado and Prinn*, 2009] or performed three-dimensional Eulerian simulations [*Trentmann et al*., 2003; *Alvarado et al*., 2009], the LPCS-REAM model simulated the cross section of a fire plume along the cross-wind direction, so as to capture the strong concentration gradient within the plume. The cross section was discretized into 200 horizontal boxes, each 50 m wide. Both the photochemistry within individual boxes and the mixing among different boxes were computed alternately at a 15 s time step. The gas phase O_3-NO_x-hydrocarbon photochemistry mechanism was taken from the 1-D REAM, including 110 species and 400 reactions. Chemical kinetics data were updated following the latest compilation by *Sander et al*. [2011]. Additionally, the model implemented a new isoprene chemistry mechanism based on *Paulot et al*. [2009a] and *Paulot et al*. [2009b]. In our case, the use of the updated isoprene mechanism led to negligible differences for the species of interest (e.g., O_3 and PAN). The model used an implicit diffusion scheme to calculate the mixing process along the cross-wind direction [*Zhang et al*., 2014]. The dilution parameters included the initial plume width and the cross-wind horizontal diffusion coefficient, K_y. The initial plume widths for all cases were set as 500 m, consistent with the typical field size observed during SEAC[4]RS, and were represented by the center 10 boxes in the model (the 96th–105th boxes). K_y was determined through a pretest, in which the model was run with various K_y (100, 500, 1000, 2000, 4000, 6000, and 10000 $m^2 s^{-1}$). When a plume was penetrated by the aircraft more than one time (Table 2), it was likely that the dilution conditions had changed and thus each pass was simulated separately. For each long-axis pass, we chose the K_y with which the simulated CO concentrations had the least sum of squared error compared with the peak-averaged CO observations. A sensitivity test confirmed that the chemical production of CO in the plume was <5%, thus negligible.

The model was constrained by aircraft measurements. Meteorological parameters such as temperature and humidity in situ observations were used as model inputs. Photolysis frequencies were calculated from measured actinic flux and laboratory-determined molecular cross sections and quantum yields [*Shetter and Müller*, 1999]. The initial concentrations in the center 10 boxes were set as fire emissions, i.e., the highest values measured in plumes near the fire sources. Note that in addition to the fast measurements, VOC data measured by WAS coupled with gas chromatography were also used as best estimates of the initial VOC emissions (Table 1). However, since WAS collected integrated air samples, the WAS VOC data tended to underestimate the actual fresh emissions. For other boxes, the initial values were specified with background concentrations. During mixing and aging processes, the boundary conditions (the 1st and 200th boxes) were specified with the background values identified from the data set. The simulated results at different plume ages were averaged from the center 25 boxes to compare with the peak-averaged measurements. Two examples of simulated CO mixing ratios along the cross-wind direction at ages between 0 and 30 min are shown in Figure S4.

To understand how VOC, oxygenated volatile organic compound (OVOC), and HONO emissions from the agricultural fires impact the production of PAN, a series of sensitivity tests were conducted by perturbing initial concentrations. Specifically, the sensitivities of PAN production to acetaldehyde, propene, isoprene, methylglyoxal, methyl ethyl ketone (MEK), diacetyl, and HONO emissions were examined. Since HONO and several important PAN precursors including methylglyoxal, MEK, and diacetyl [*Liu et al*., 2010] were not measured in the campaign, the EFs for rice straw measured by *Stockwell et al*. [2015] were applied in order to estimate their initial concentrations by scaling with the observed CO.

In addition to gaseous species, nitrate, SOA, and the O/C ratios were also modeled. We estimated the nitrate production through the deposition of nitric acid (HNO_3) to the aerosol surface using the formulation by *Dahneke* [1983], with an uptake coefficient assigned as 0.15 [*Sander et al*., 2011]. The aerosol surface area was calculated based on measurements by a laser aerosol spectrometer (TSI Inc., St. Paul, MN). Dry deposition velocity of HNO_3 was set as 2 cm s^{-1} [*Zhang et al*., 2009]. The wet deposition of HNO_3 and the dry/wet deposition of nitrate aerosols to land or clouds were not included in the simulation because of the short time span of the simulation (~1 h) and the common clear-sky conditions during the flights of interest. The SOA production was calculated following the simple parameterization by *Hodzic and Jimenez* [2011], using a mass emission ratio of 0.013 g of a lumped SOA precursor per gram of CO based on *Cubison et al*. [2011], a SOA yield of one, and a rate constant with hydroxyl radical (OH) of 1.25×10^{-11} cm^3 $molecule^{-1}$ s^{-1}. Deriving the photochemical age from the simulated OH concentrations, the evolution of the O/C ratios of primary organic aerosol (POA) was also calculated with the following equation similar to the approach proposed by *Hodzic and Jimenez* [2011] for the evolution of urban emissions, but with different parameters

$$O/C = 0.6 - 0.2exp\left(-\frac{A}{0.05}\right) \quad (7)$$

where A is days of photochemical age computed by dividing OH exposure by a typical OH concentration of 1.5×10^6 molecules cm^{-3}, i.e., $A = \left(\int_0^t [OH]dt\right)/\left(1.5\times10^6 \text{molecules } cm^{-3}\right)$, and 0.05 in days is the aging time scale for the agricultural fires.

Due to plume tracking difficulties, plume intercepts were rarely perfect, posing challenges to model simulation. To realistically interpret the photochemical processes, the cases presented here were selected because (1) the dilution could be reasonably simulated with the model; (2) there are enough downwind data to compare with the modeled concentrations; and (3) the initial concentrations of important species, such as NO_x, are available. These cases include the second pass of Fire 3, the two passes of Fire 4, and the first and third passes of Fire 15.

3. Results

3.1. Initial Emissions

The average MCEs and EFs for the 15 agricultural fires are shown in Table 3 along with the study-averaged MCE and EF. Among the species that were quantified by the fast measurements from the NASA DC-8 platform, at least 25 trace gases and 6 particle species exhibited elevated concentrations within the agricultural fire plumes. This represents the most comprehensive suite of species measured in the field in the U.S. for

Table 3. Measured MCE and Emission Factors (g/kg) for All Agricultural Fires Sampled During SEAC[4]RS in Summer 2013[a]

Fire #		1	2	3	4	5	6	7	8
Date		6 Sep	9 Sep	9 Sep	11 Sep	16 Sep	16 Sep	16 Sep	16 Sep
MCE		0.895	0.919	0.914	0.906	0.920	0.944	0.930	0.939
Compound	Formula								
Gases									
Carbon dioxide	CO_2	1289	1323	1316	1305	1325	1360	1340	1353
Carbon monoxide	CO	96.2	74.3	79.2	86.1	73.2	51.2	63.8	55.5
Nitrogen monoxide	NO	0.327	0.0613	0.0456	0.169	0.266	0.0904	0.118	0.125
Nitrogen dioxide	NO_2	1.79	1.38	1.84	2.09	1.37	0.718	1.73	2.23
Hydrochloric acid	HCl	0.0207	0.00497	0.0253	0.0619	0.00792		0.0143	0.00545
Sulfur dioxide	SO_2	0.807	0.334	0.698	1.11	0.228		0.792	0.863
Hydrogen cyanide	HCN	0.350		0.789	2.02	0.414	0.316	0.826	0.186
Formaldehyde	HCHO	4.14	2.14	3.19	4.81	4.11	1.85	3.08	1.68
Methanol	CH_3OH	4.10	3.83	1.36	0.725	0.785	0.865	0.545	0.0566
Hydroxyacetone	$C_3H_6O_2$	2.59		3.56	3.93	2.35	1.61	1.70	1.06
Acetonitrile	CH_3CN	0.300	0.456	0.221	0.179	0.0535	0.0627	0.210	0.0638
Acetaldehyde	C_2H_4O	1.46	2.66	2.02	1.43	1.19	0.812	3.00	0.948
Acetone/propanal	C_3H_6O	0.555	1.697	1.12	0.329	0.436	0.439	0.893	0.0787
MVK/MACR/crotonaldehyde	C_4H_6O	0.773	0.612	0.661	1.17	0.285	0.252	0.528	0.234
Isoprene/pentadienes/cyclopentene/furan	C_5H_8/C_4H_4O	0.651	0.910	0.820	0.0501	0.279	0.238	0.648	0.0661
Isoprene hydroperoxyaldehydes	$C_5O_3H_8$	0.975		0.684	0.710	0.330	0.243	0.263	0.235
Benzene	C_6H_6	0.320	0.360	0.313	0.657	0.177	0.160	0.373	0.207
Monoterpenes[b]	C_6H_8	0.530	0.197	0.546	0.357	0.155	0.160	0.404	0.159
Toluene[c]	C_7H_8	0.355	0.224	0.211	0.284	0.0986	0.0871	0.250	0.0919
Particles									
Ammonium	NH_4	0.509	0.0745	0.813	0.995	0.151	0.133	0.364	
Nitrate	NO_3	0.441	0.283	0.326	0.419	0.398	0.316	0.425	
Chloride	Chl	1.30	0.323	2.37	3.23	0.132	0.138	0.715	
Sulfate	SO_4	0.420	-0.026	0.139	0.199	0.361	0.111	0.146	
Organic aerosol	OA	13.4	8.20	18.5	20.9	27.6	4.15	9.10	
Black carbon	BC	0.270	0.209	0.059	0.106	0.024	0.027	0.192	0.316
Submicron aerosol[d]	PM_1	16.3	9.06	22.2	25.8	28.6	4.88	10.9	

[a]The study averages and the standard deviations are indicated in bold. Blank indicates no measurement available for the fire.
[b]Measured by PTR-MS at *m/z* 137 and calibrated using α-pinene. By burning rice straw in a laboratory experiment, *Stockwell et al.* [2015] found up to two additional peaks at *m/z* 137 that were oxygenated compounds. However, *Müller et al.* [2016] did not find a significant contribution from oxygenated compounds to this signal from forest fuel.
[c]Measured by PTR-MS at *m/z* 93. *Müller et al.* [2016] found a 20% interference from the $C_6H_5O^+$ signal.
[d]Sum of AMS species and BC.

agricultural fires to date. The fire-integrated MCEs derived in this work range from 0.895 to 0.958, with an average of 0.930. Hence, most of these fires can be regarded as primarily flaming. EFs for most species depend on the MCE. For this reason, we examined the calculated MCE and its correlation with EFs. Table 4 shows the linear regression results of EFs as a function of MCE for all species, including slopes, *y* intercepts, and r^2. No species had a good correlation ($r^2 > 0.1$) and a positive slope significantly different from zero, which would signify production mainly by flaming combustion. Compounds with negative slopes are likely associated with smoldering combustion since the emissions increase as the MCE decreases (e.g., toluene and benzene). However, numerous factors besides flaming and smoldering could dominate the variability in EFs. For species containing elements other than carbon, hydrogen, or oxygen, the emissions can depend strongly on the fuel composition (e.g., SO_2 and NO_x) [*Burling et al.*, 2010]. In general, the EFs of organic gases correlated better with MCE than the EFs of inorganic gases and particles. The SEAC[4]RS EFs were also compared to the limited crop residue burning EFs available from the literature, including both field and laboratory studies. Table 5 summarizes the average EFs, the crop residue fuels burned, and the measurement approach (i.e., field or lab study) for these studies. Note that the EFs from *Stockwell et al.* [2015] are predicted EFs at the SEAC[4]RS-averaged MCE based on their linear regression between EF and MCE.

3.1.1. Emissions of Sulfur Compounds

Sulfur in soil partly comes from atmospheric deposition and is then made available to plants by bacterial activity [*Wilhelm Scherer*, 2009]. Another source of soil sulfur is S fertilization, which helps increase rice yield

Table 3. (continued)

Fire #		9	10	11	12	13	14	15		
Date		16 Sep	16 Sep	23 Sep	23 Sep	23 Sep	23 Sep	23 Sep	Average	Standard Deviation
MCE		0.926	0.947	0.957	0.958	0.922	0.942	0.926	**0.930**	**0.018**
Compound	Formula									
Gases										
Carbon dioxide	CO_2	1334	1364	1378	1379	1328	1356	1334	**1339**	**26**
Carbon monoxide	CO	67.4	48.4	39.7	38.8	71.5	53.6	67.9	**64.5**	**16.6**
Nitrogen monoxide	NO	0.179	0.285	0.111	0.444	0.244	0.435	0.863	**0.251**	**0.211**
Nitrogen dioxide	NO_2	3.41	3.37		1.32		2.22	2.85	**2.02**	**0.80**
Hydrochloric acid	HCl		0.0131	0.0206	0.0162	0.0167	0.0158	0.0129	**0.0181**	**0.0144**
Sulfur dioxide	SO_2		1.70	1.08	0.407	0.730	0.818	0.767	**0.795**	**0.377**
Hydrogen cyanide	HCN	0.823	0.308	0.334	0.308	0.532	0.339	0.990	**0.610**	**0.479**
Formaldehyde	HCHO	2.26	1.64	1.90	1.49	3.09	2.02	1.97	**2.63**	**1.05**
Methanol	CH_3OH		3.55	1.01	1.54	0.952	0.118	0.335	**1.41**	**1.38**
Hydroxyacetone	$C_3H_6O_2$	1.60	0.838	1.46	2.61	2.21	1.32	1.95	**2.06**	**0.89**
Acetonitrile	CH_3CN		0.324	0.0955	0.0978	0.170	0.0281	0.105	**0.169**	**0.123**
Acetaldehyde	C_2H_4O		0.749	0.998	0.456	2.11	0.408	0.921	**1.37**	**0.80**
Acetone/propanal	C_3H_6O		0.923	0.433	0.375	0.806	0.296	0.551	**0.638**	**0.417**
MVK/MACR/crotonaldehyde	C_4H_6O		0.0266	0.256	0.201	0.618	0.162	0.501	**0.449**	**0.305**
Isoprene/pentadienes/ cyclopentene/furan	C_5H_8/C_4H_4O		0.195	0.261	0.221	0.674	0.253	0.491	**0.411**	**0.282**
Isoprene hydroperoxyaldehydes	$C_5O_3H_8$	0.298	0.214	0.246	0.469	0.440	0.287	0.285	**0.406**	**0.229**
Benzene	C_6H_6		0.132	0.202	0.121	0.327	0.199	0.295	**0.275**	**0.139**
Monoterpenes[b]	C_6H_8		0.236	0.0636	0.114	0.398	0.0360	0.256	**0.258**	**0.164**
Toluene[c]	C_7H_8		0.184	0.0714	0.0872	0.160	0.0487	0.184	**0.167**	**0.091**
Particles										
Ammonium	NH_4	0.348	0.582	0.355	0.234	0.612	0.341	0.420	**0.424**	**0.261**
Nitrate	NO_3	0.229	0.168	1.22	0.0792	1.16	0.414	0.228	**0.436**	**0.337**
Chloride	Chl	1.07	1.66	0.176	1.22	0.883	0.555	1.16	**1.07**	**0.89**
Sulfate	SO_4	0.102	0.115	0.184	0.0932	0.210	0.0504	0.135	**0.160**	**0.115**
Organic aerosol	OA	8.81	7.02	11.0	10.8	18.0	11.0	12.2	**12.9**	**6.3**
Black carbon	BC	0.521	0.226	0.158	0.049	0.037		0.082	**0.163**	**0.141**
Submicron aerosol[d]	PM_1	11.1	9.77	13.1	12.5	20.9		14.2	**15.4**	**7.1**

[*Tsujimoto et al*., 2013]. Significant amounts of SO_2 and sulfate were observed in the sampled fire plumes, up to 80 ppbv and 15 ppbv (Figure S2), respectively. As can be seen from Table 3, the excess mixing ratios of SO_2 are substantially higher than those of sulfate. This indicates that the emitted sulfur was mainly in the form of gaseous SO_2. The average EF(SO_2) for SEAC^{4}RS is 0.795 ± 0.377 g/kg, which is nearly 2 times higher than the existing EF(SO_2) for several other types of BB including tropical forest, savanna, and pasture maintenance fires [*Akagi et al*., 2011]. This implies high sulfur content in rice straw, possibly resulting from high sulfur input into soil such as S fertilization or high absorption of sulfur by rice. When compared to the lab-predicted EF(SO_2) for Asian rice straw [*Stockwell et al*., 2015], 1.22 ± 0.34 g/kg, the field average EF for U.S. rice straw is lower, statistically significant based on *t* test at a 95% confidence level. The differences between the lab-predicted EF (SO_2) and the field EF(SO_2) could be due to the differences in fuel, burning conditions, and sampling methods. SO_2 has been established previously as a product of flaming combustion [*Yokelson et al*., 1996; *Andreae and Merlet*, 2001]. For the agricultural fires sampled during SEAC^{4}RS, although the slope of the linear fit of EF(SO_2) as a function of MCE is positive, the low r^2 with a value of 0.05 indicates that the amount of emitted SO_2 was not primarily dependent on the ratio of flaming to smoldering. It is likely that SO_2 emissions are highly dependent on fuel sulfur content, as also found in laboratory studies [*Burling et al*., 2010; *Stockwell et al*., 2014]. For particulate sulfate emissions, the average EF is 0.160 ± 0.115 g/kg. *Hayashi et al*. [2014] measured lower EF(sulfate) from Japanese rice straw with values of 0.027 ± 0.000 and 0.063 ± 0.003 g/kg under different residue moisture contents of 10.6% and 20.0%, respectively. The average EF(sulfate) during SEAC^{4}RS is over 2 times higher than those measured by *Hayashi et al*. [2014], probably due to fuel variability.

Table 4. Statistics for the Linear Regression of Fire-Averaged EF as a Function of Fire-Integrated MCE[a]

Species	Slope	Y Intercept	r^2
Species With Positive Slopes Not Significantly Different From 0			
SO_2	4.25 (5.83)	−3.16 (5.42)	0.05
NO_x as NO	2.6 (10.8)	−0.82 (9.99)	0.005
NO	0.69 (3.23)	−0.39 (3.00)	0.004
Nitrate	0.98 (5.23)	−0.48 (4.86)	0.003
NO_2	1.1 (13.7)	1.0 (12.7)	0.0005
Species With Negative Slopes Significantly Different From 0			
MVK/MACR/crotonaldehyde	−13.4 (2.7)	12.9 (2.5)	0.68
HCHO	−47.7 (9.3)	47.0 (8.6)	0.67
Toluene	−3.88 (0.85)	3.78 (0.79)	0.64
Monoterpenes	−6.66 (1.64)	6.45 (1.53)	0.58
HPALDs	−9.33 (2.35)	9.09 (2.19)	0.57
$\Delta b_{ap,BrC}(365)/(\Delta CO + \Delta CO_2)$[b]	−0.226 (0.059)	0.226 (0.055)	0.53
Benzene	−5.17 (1.54)	5.08 (1.43)	0.48
Hydroxyacetone	−30.5 (10.8)	30.5 (10.1)	0.40
Species With Negative Slopes Not Significantly Different From 0			
HCN	−13.4 (6.4)	13.0 (6.0)	0.27
Acetaldehyde	−21.9 (10.6)	21.8 (9.8)	0.26
OA	−173 (84)	173 (78)	0.26
Sulfate	−3.06 (1.56)	3.01 (1.45)	0.24
Isoprene/furan/pentadienes/cyclopentene	−7.35 (3.79)	7.24 (3.52)	0.24
Ammonium	−6.06 (3.66)	6.05 (3.40)	0.19
CH_3CN	−2.81 (1.72)	2.79 (1.60)	0.18
Chloride	−20.4 (12.5)	20.0 (11.7)	0.18
HCl	−0.274 (0.213)	0.273 (0.198)	0.13
CH_3OH	−20.9 (20.3)	20.8 (18.9)	0.08
Acetone/propanal	−6.18 (6.17)	6.39 (5.74)	0.08
BC	−0.54 (2.19)	0.67 (2.04)	0.005

[a]Values in parentheses represent one standard deviation. Species are organized by the sign and significance of slopes and then by the magnitude of r^2.
[b]The unit of the ER of $\Delta b_{ap,BrC}(365)/(\Delta CO + \Delta CO_2)$ is Mm^{-1} ppb^{-1}.

3.1.2. Emissions of Chlorine Compounds

Sea salt deposition and the use of agricultural chemicals such as herbicides and insecticides can increase the chlorine content in plants and therefore chlorine emissions from BB. The chlorine-containing species quantified in this study are gaseous HCl and particulate chloride. For the 15 fires we sampled, average EFs of chloride and HCl are 1.07 ± 0.89 and 0.0181 ± 0.0144 g/kg, respectively. If we calculate the average molar ratio of emitted chloride to HCl from their average EFs, a ratio of ~60 indicates that chlorine was mainly emitted as chloride. Since the samples were all from inland areas, the high chloride emission from rice straw burning are more likely to result from the use of agricultural chemicals rather than impacts from sea salt. During FLAME-4, *Stockwell et al*. [2014] observed high HCl emissions with an average EF of 0.458 ± 0.308 g/kg, adjusted to the SEAC^{4}RS-averaged MCE. They also observed that the concentration of HCl decayed rapidly in several minutes in fresh smoke that was stored in low-light conditions for rice straw and other fuels. *Christian et al*. [2010] observed high chloride and below-detection-limit HCl in the fresh emissions from two barley residue fires in Mexico. *Stockwell et al*. [2014] obtained fresher samples in the lab, which were seconds old, while this study and *Christian et al*. [2010] sampled smoke that was usually several minutes old in field. Thus, the reason that the field studies observed much less HCl might be that HCl rapidly decreased after emission by partitioning to the aerosol phase. In the lab study conducted by *Hayashi et al*. [2014], fire-integrated samples of HCl and chloride were collected by cellulose filters and glass-fiber filters, respectively. Therefore, the observed high chloride and low HCl EFs were averages from a complete burning process from the ignition to the end of the smoldering period.

Lab studies have shown that the emission of HCl correlates with flaming combustion [*Burling et al*., 2010; *Stockwell et al*., 2014], while that of particulate chloride does not depend strongly on the ratio of flaming to smoldering [*Christian et al*., 2003]. However, for the U.S. rice straw, the linear fits of EFs versus MCEs in

Table 5. Comparison of EFs (g/kg) Measured in Field and Lab for Crop Residue Fuels[a]

Compound	SEAC[4]RS (This Work)	FLAME-4 at SEAC[4]RS-Average MCE (*Stockwell et al.* [2015])	*Akagi et al.* [2011][b]	*Kudo et al.* [2014][c]	*Hayashi et al.* [2014]	
Crop type	SE U.S. rice straw	Asian rice straw	Unidentified crop residue in Mexico	Chinese wheat	Japanese rice straw	
Measurement approach	Airborne field study	Lab study	Airborne field study	Ground-based field study	Lab study	
Moisture content (%)	-	-	-	-	10.6	20.0
MCE	0.930	0.930	0.925	0.930	0.949	0.910
CO_2	1339 (26)	-	1664 (66)	1598 (5)	803 (65)	946 (49)
CO	64.46 (16.57)	-	85.6 (34)	77.2 (6.9)	27.2 (1.7)	59.4 (0.7)
NO	0.251 (0.211)	1.86 (0.28)	2.06 (0.79)	-	-	-
NO_2	2.02 (0.80)	1.70 (0.25)	3.48 (2.11)	-	-	-
NO_x as NO	1.58 (0.63)	2.97 (0.32)	3.64 (1.13)	-	-	-
NH_3	-	1.12 (0.77)	1.76 (1.35)	-	0.059 (0.045)	0.025 (0.020)
HCl	0.0181 (0.0144)	0.458 (0.308)	-	-	0.062 (0.003)	0.022 (0.006)
SO_2	0.795 (0.377)	1.22 (0.34)	-	-	-	-
HCN	0.610 (0.479)	0.399 (0.160)	0.16 (0.30)	-	-	-
HCHO	2.63 (1.05)	1.29 (0.61)	1.85 (0.92)	1.07	-	-
CH_3OH	1.41 (1.38)	1.48 (1.56)	2.67 (1.58)	2.94	-	-
Hydroxyacetone	2.06 (0.89)	1.33 (1.47)	-	-	-	-
CH_3CN	0.169 (0.123)	0.230 (0.092)	-	0.20 (0.03)	-	-
Acetaldehyde	1.37 (0.80)	2.09 (1.46)	-	1.02	-	-
Acetone	0.638 (0.417)[d]	0.989 (0.532)	-	0.83[d]	-	-
Propanal		-	-		-	-
MVK	0.449 (0.305)[f]	0.489 (0.398)[e]	-	0.43 (0.02)[e]	-	-
MACR			-		-	-
Crotonaldehyde		-	-	-	-	-
Isoprene	0.411 (0.282)[h]	0.203 (0.104)	-	0.52 (0.01)[g]	-	-
Furan		0.325 (0.496)	-		-	-
Pentadienes		-	-	-	-	-
Cyclopentene		-	-	-	-	-
HPALDs	0.406 (0.229)	-	-	-	-	-
Benzene	0.275 (0.139)	0.302 (0.123)	-	0.53 (0.07)	-	-
Monoterpenes	0.258 (0.164)	-	-	-	-	-
Toluene	0.167 (0.091)	0.271 (0.138)	-	0.32	-	-
Ammonium	0.424 (0.261)	-	-	-	0.083 (0.020)	0.245 (0.092)
Nitrate	0.436 (0.337)	-	-	-	0.006 (0.002)	0.008 (0.000)
Chloride	1.07 (0.89)	-	-	-	0.30 (0.02)	0.69 (0.14)
Sulfate	0.160 (0.115)	-	-	-	0.027 (0.000)	0.063 (0.003)
OA	12.9 (6.3)	-	3.67[i]	-	1.6[j]	7.4[j]
BC	0.163 (0.141)	-	0.75	-	-	-

[a]Values in parentheses represent one standard deviation.
[b]Supplement Table 13 in *Akagi et al.* [2011].
[c]The EFs in *Kudo et al.* [2014] were derived from two plumes. The values in parentheses are the ranges of data.
[d]EF for acetone/propanal.
[e]EF for MVK/MACR.
[f]EF for MVK/MACR/crotonaldehyde.
[g]EF for isoprene/furan.
[h]EF for isoprene/furan/pentadienes/cyclopentene.
[i]The average OA from *Yokelson et al.* [2009] (Table 3) from Fires 1 and 3.
[j]Derived from EF(OC) times a factor of 1.64 [*Canagaratna et al.*, 2015].

Table 4 indicate that neither HCl nor chloride strongly correlates with MCE ($r^2 \leq 0.18$). Analogous to sulfur, EFs of chlorine species are likely highly dependent on the fuel composition. *Christian et al.* [2003] and *Hosseini et al.* [2013] found a strong relationship between fuel chlorine content and chloride-containing particulate emissions for a series of laboratory fires. *Stockwell et al.* [2014] also found in lab studies that for a wide variety of biomass fuels, the emissions of HCl were positively correlated with fuel Cl. In this airborne study, a large fraction of HCl may have already incorporated into the particles before being sampled, which could also lead to a weak correlation between EF(HCl) and MCE.

3.1.3. Emissions of Nitrogen Compounds

BB is an important atmospheric source of nitrogen species, primarily NH_3 and NO_x [*Crutzen and Andreae*, 1990; *McMeeking et al*., 2009; *Burling et al*., 2010]. Freshly emitted nitrogen-containing compounds measured during SEAC^{4}RS are HCN, CH_3CN, NO_x, nitrate, and ammonium. Another important nitrogen species not measured during SEAC^{4}RS could be HONO. Significant direct emissions of HONO were reported at ~5–33% of NO_x from BB of various fuel types [*Yokelson et al*., 2007, 2009; *Burling et al*., 2011; *Akagi et al*., 2012, 2013] and at ~9% of NO_x for Asian rice straw burned in lab [*Stockwell et al*., 2015]. Thus, HONO emission could be an important source of OH radicals. HCN and CH_3CN are widely recognized as useful BB tracers [*Li et al*., 2000; *de Gouw et al*., 2003; *Li et al*., 2003]. The variability in HCN emissions is significant over a broad range of fuel types [*Akagi et al*., 2011]. HCN from crop residue fires has previously been measured in the laboratory and in field studies in Mexico [*Christian et al*., 2003; *Akagi et al*., 2011; *Stockwell et al*., 2014]. These measurements show that the average EF(HCN) for SEAC^{4}RS rice straw fires is the largest among these crop residue fires with a value of 0.610 ± 0.479 g/kg (Table 5). This EF(HCN) is also slightly larger than those for other types of BB except forest fires and peat as reviewed in *Akagi et al*. [2011]. In general, airborne and ground-based EF(HCN) for pine/conifer fuels show a strong negative correlation with MCE over a wide range of 0.85–0.96, suggesting that HCN is primarily released from smoldering combustion [*Akagi et al*., 2013]. By contrast, no statistically significant linear dependence of airborne EF(HCN) on MCE was detected in this work (Table 4). Airborne HCN EFs measured in some other studies of "nonpine" ecosystems, e.g., African savanna fires [*Yokelson et al*., 2003], are also effectively independent of MCE. The emission of CH_3CN is lowest among all the nitrogen-containing species (Table 3). The average EF(CH_3CN) reported here is smaller than those reported in the literature for crop residues (Table 5), although not statistically significant. The EF(CH_3CN) for individual fires ranges from 0.0281 to 0.456 g/kg and is weakly correlated with MCE (Table 4). The study-averaged ER of $\Delta CH_3CN/\Delta HCN$ is 0.22 ± 0.20, smaller than previous laboratory and field measurements of 0.30–0.56 for a wide range of nonboreal [*Christian et al*., 2003; *Yokelson et al*., 2008; *Crounse et al*., 2009; *Yokelson et al*., 2009] and boreal [*Simpson et al*., 2011] fuel types.

In this study, the average EF(NO_2), 2.02 ± 0.80 g/kg, is approximately 8 times the average EF(NO), 0.251 ± 0.211 g/kg. This NO_2/NO ratio, largely controlled by photostationary state, is the largest among the crop residue studies listed in Table 5. Since NO and NO_2 are rapidly interconverted, it is also useful to report an EF for "NO_x as NO." The EF(NO_x) of this study is 1.58 ± 0.63 g/kg, the smallest among the studies listed in Table 5. As for the EF(NO_x) versus MCE plots, although some laboratory and field measurements have shown that NO_x is emitted primarily via flaming combustion [*Lobert et al*., 1991; *Yokelson et al*., 1996; *Goode et al*., 2000], neither EF(NO), EF(NO_2), nor EF(NO_x) from SEAC^{4}RS correlates with MCE (Table 4). Instead, NO_x emissions might have been driven more by fuel nitrogen content than MCE, as found in *Burling et al*. [2010], *Andreae and Merlet* [2001], and *McMeeking et al*. [2009]. However, since SEAC^{4}RS agricultural fires emitted less NO_x and CH_3CN but more HCN, it is likely that the emissions of gaseous nitrogen compounds depend not only on the total fuel nitrogen but also the composition of N-containing precursors in fuel and burning conditions [*Becidan et al*., 2007; *Bai et al*., 2013]. Gaseous HNO_3 was not significantly elevated within most of the fire plumes. Other studies have reported that HNO_3 did not correlate with elevated CO within fresh or aged BB smoke [*Yokelson et al*., 2009; *Alvarado et al*., 2010]. The reason for this may be that HNO_3 is converted efficiently to nitrate due to the availability of NH_3 in the plumes, as indicated by high ammonium emissions. The evolution of nitrogen species will be discussed in detail in section 3.2.2.

Particulate nitrate and ammonium are often minor components of the emitted nitrogen species. *Akagi et al*. [2011] reviewed the emissions of these particles in various BB types. The observed nitrate EFs ranged from 0.016 to 0.14 g/kg, and those of ammonium were smaller than 0.006 g/kg. *McMeeking et al*. [2009] also found particulate nitrate and ammonium to account for only a small fraction of the fuel nitrogen for 33 different U.S. plant species and rice straw collected from Taiwan burned in a lab study. Their study-averaged values of EF (nitrate) and EF(ammonium) for rice straw were 0.04 ± 0.03 g/kg and 0.26 ± 0.16 g/kg, respectively. *Hayashi et al*. [2014] also observed very low emissions of nitrate and relatively higher emissions of ammonium under both dry and moist conditions (Table 5). During SEAC^{4}RS, fresh nitrate and ammonium emissions with average EFs of 0.436 ± 0.337 g/kg and 0.424 ± 0.261 g/kg were measured, respectively, which are larger than the existing literature values. In addition, both nitrate and ammonium exhibited enhancement in aged smoke. If the initial emitted and subsequently produced nitrate and ammonium are summed, both nitrate and ammonium would have even higher emissions than the lab studies of *McMeeking et al*. [2009] and *Hayashi et al*. [2014].

3.1.4. Emissions of Gas Phase Nonmethane Organic Compounds (NMOCs)

Among the reported gas phase NMOCs, rice straw fires had the highest average EFs for formaldehyde, hydroxyacetone, methanol, and acetaldehyde. In previous studies, formaldehyde is consistently one of the most abundant OVOCs emitted by fires [*Goode et al*., 2000; *Yokelson et al*., 2003]. The field burning of U.S. rice straw produced significant amounts of formaldehyde with an average EF of 2.63 ± 1.05 g/kg, which is the largest EF among all types of BB shown in Table 5 and in *Akagi et al*. [2011], except charcoal making.

Hydroxyacetone has both biogenic and BB sources. It is the precursor of other atmospherically important species, such as methyglyoxal, formic acid, and acetic acid [*Grosjean et al*., 1993; *Butkovskaya et al*., 2006]. Hydroxyacetone emissions have recently been reported for both field and laboratory fires from various fuels [*Christian et al*., 2003; *Akagi et al*., 2011; *Yokelson et al*., 2013; *St. Clair et al*., 2014]. *Christian et al*. [2003] reported very large quantities of hydroxyacetone, 21–34 g/kg, from burning Indonesian rice straw in piles under smoldering combustion (a common practice in Indonesia and East Asia) with a MCE of ~0.81. Rice straw burned in FLAME-4 also had a relatively high average EF (1.33 ± 1.47 g/kg) for the SEAC^{4}RS-averaged MCE value. The fires sampled during the SEAC^{4}RS also produced high amounts of hydroxyacetone with an average EF of 2.06 ± 0.89 g/kg.

In SEAC^{4}RS and previous studies, methanol was consistently one of the most abundant OVOCs emitted by crop residue fires and other types of BB [*Christian et al*., 2003; *Kudo et al*., 2014; *Stockwell et al*., 2014, 2015]. The SEAC^{4}RS and the FLAME-4 lab-predicted EFs of methanol agree very well (Table 5).

Acetaldehyde plays an important role in the formation of PAN, O_3, and HO_x radicals and also has large effects on modeled smoke plume chemistry [*Singh et al*., 1995; *Trentmann and Andreae*, 2003; *Trentmann et al*., 2005]. The annual emission of acetaldehyde from BB has been estimated as 3 Tg [*Millet et al*., 2010]. As the principal carbonyl precursor of PAN (44% of the global source) [*Fischer et al*., 2014], acetaldehyde emitted from BB likely has an important impact on the regional and global PAN budget. Burning crop residues emits relatively large amounts of acetaldehyde relative to other types of fuel. Among the five types of crop residues burned in FLAME-4, sugar cane and rice straw had the largest acetaldehyde EFs [*Stockwell et al*., 2015]. We report an average EF (acetaldehyde) of 1.37 ± 0.80 g/kg, which is smaller than that measured in FLAME-4 [*Stockwell et al*., 2015], though the uncertainties are large (Table 5). The impact of acetaldehyde emissions on PAN formation in aged smoke is studied in detail by the LPCS-REAM model and is discussed in section 3.3.

Other quantified organic gases include (in order of abundance by mass): acetone/propanal, MVK/MACR/crotonaldehyde, isoprene/furan/pentadienes/cyclopentene, isoprene hydroperoxyaldehydes (HPALDs), benzene, monoterpenes, CH_3CN, and toluene. Among these species, the OVOCs are relatively abundant initial emissions from BB. HPALDs are autoxidation products of isoprene via 1,6-H-shift isomerizations of peroxy radicals produced from OH + isoprene [*Crounse et al*., 2011, 2013]. Their production is expected to be important in low-temperature combustion chemistry as occurs in BB [*Cox and Cole*, 1985; *Rogge et al*., 1991]. The first direct emissions of HPALDs from BB were measured during SEAC^{4}RS, with an average EF of 0.406 ± 0.229 g/kg. For those overlapping species in Table 5, the average EFs of our field study and those predicted from the FLAME-4 EF versus MCE plot are shown to agree well, considering the differences in fuel and burning conditions. There were larger discrepancies in the NMOC EFs derived in this work as compared to those in *Kudo et al*. [2014], although the average MCEs were similar. In general, *Kudo et al*. [2014] obtained higher EFs, perhaps because of the difference in the composition of wheat and rice straw.

The emissions of all the NMOCs are negatively correlated with MCE (Table 4), meaning they are primarily emitted from smoldering combustion. However, variability in the relationship between EFs and MCE does exist. MVK/MACR/crotonaldehyde, toluene, monoterpenes, and HPALDs correlate reasonably well with MCE (r^2 from 0.57 to 0.68). On the other hand, acetone/propanal and methanol are the NMOCs that were least dependent on MCE, both with $r^2 = 0.08$. The acetone/propanal and MCE correlation is reported for the first time here. For methanol, unlike in this study, good correlation (r^2 from 0.68 to 0.90) between the EF (methanol) and MCE has been reported in previous lab and field studies focusing on the fuels burned in prescribed and savanna fires [*Christian et al*., 2003; *Yokelson et al*., 2003; *Burling et al*., 2010, 2011].

3.1.5. Emissions of Carbonaceous Aerosols

Open BB, as a primary source of carbonaceous aerosols, contributes one third of the global BC and two thirds of the global POA budget [*Bond et al*., 2004]. BC is known to be the most absorbing aerosol in the visible wavelengths in the atmosphere [*Bond et al*., 2013]. Recent studies have shown that BB OA contains substantial amounts of light-absorbing BrC [*Kirchstetter et al*., 2004; *Chen and Bond*, 2010; *Lack et al*., 2012;

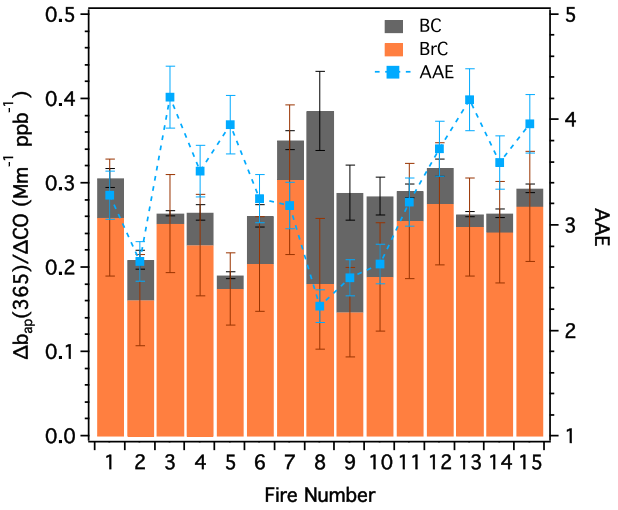

Figure 4. Excess PSAP light absorption coefficient at 365 nm normalized by excess CO and corresponding absorption Ångström exponent (AAE) in fresh smoke. BrC absorption was 2–5 times that of BC at 365 nm.

Saleh et al., 2013; *Washenfelder et al.*, 2015]. EFs and chemical properties of BC and OC from BB are quite variable and uncertain [*Reid et al.*, 2005]. Here we examine the first suite of field measurements of BC and OA emitted from agricultural fires. We also use the PSAP data to infer the existence and absorption properties of BrC.

The EFs of BC in this work vary between 0.024 and 0.521 g/kg, with an average of 0.160 ± 0.115 g/kg (Table 3). This average value is ~5 times smaller than that derived from field measurement of EC from Mexican crop residue burning (Table 5) and is also smaller than the EF(BC) reviewed in *Akagi et al.* [2011] for all types of BB except charcoal making. Previous studies have shown that BC is a flaming combustion product [*Christian et al.*, 2003; *Reid et al.*, 2005]. However, our BC EFs are essentially independent of MCE (Table 4). Therefore, given the complexity and variability of biomass combustion, the variance of EF(BC) was not attributable simply to the relative amount of flaming or smoldering for the SEAC^{4}RS agricultural fire measurements.

OA comprised the largest chemical component of fine particles in smoke from the sampled agricultural fires, with an average EF of 12.9 ± 6.3 g/kg (Table 3). *Yokelson et al.* [2009] and *Hayashi et al.* [2014] observed significantly less OA emissions from crop residue fires (Table 5). Contrary to BC, OA is mainly produced by smoldering combustion [*Reid et al.*, 2005]. OA EFs are negatively correlated with MCE ($r^2 = 0.26$), as expected (Table 5). This correlation is weaker than some previously observed average EF(OC) and MCE correlations with $r^2 = 0.36$ for various plant species burned in lab [*McMeeking et al.*, 2009; *Jolleys et al.*, 2014]. It is possible that some of the variance in these OA EFs could be due to fire variability. The strength of the relationship between EF(OA) and MCE can also be degraded by gas-particle partitioning effects. POA emitted from fires has been observed to be semivolatile [*Donahue et al.*, 2006; *May et al.*, 2013]. Thus, although the samples used to calculate EF(OA) are relatively fresh, the POA may still have gone through variable gas-particle partitioning related to dilution and temperature changes as the smoke mixes with background air.

As shown in Figure 4, the calculated PSAP AAEs range from 2.2 to 4.2 near the 15 fire sources, higher than the average AAE of the background air just outside of the plumes (1.60 ± 0.40). The average AAE for the agricultural fires, 3.34 ± 0.62, is similar to the AAEs of 3.5 to 4.0 for the fresh plumes of a large wildfire, the Rim Fire, sampled during the same campaign [*Forrister et al.*, 2015]. Corresponding to the elevated AAEs, derived BrC absorption at 365 nm normalized by ΔCO was significantly elevated in all 15 fresh agricultural fire plumes, also shown in Figure 4. In contrast, the absorption at 365 nm contributed by freshly emitted BC was lower or 15%–93% of that contributed by BrC. The average fresh $\Delta b_{ap,BrC}(365)/\Delta CO$ and $\Delta b_{ap,BC}(365)/\Delta CO$ of this study are 0.223 ± 0.053 Mm^{-1} $ppbv^{-1}$ and 0.078 ± 0.036 Mm^{-1} $ppbv^{-1}$, respectively. Direct measurements of light absorption spectra from liquid extracts of aerosols collected on 20 teflon filters were also available for these agricultural fires. After applying a factor of 2 for conversion of light absorption from liquid solution to particles [*Liu et al.*, 2013, 2015; *Washenfelder et al.*, 2015], the average $\Delta b_{ap,BrC}(365)/\Delta CO$ determined from liquid extracts is 0.25 ± 0.27 Mm^{-1} $ppbv^{-1}$, which agrees with the average derived from PSAP measurements. The uncertainty of the extract-derived $\Delta b_{ap,BrC}(365)/\Delta CO$ by particles is estimated to be at least ~45% by combining the uncertainties in the conversion factor [*Liu et al.*, 2013] and the measurements. The real uncertainty is likely larger because the background absorption near the plume often cannot be obtained due to the low sampling frequency of 5–7 min. By performing orthogonal distance regression for the sum of $b_{ap,BrC}(365)$ determined from liquid extracts and $b_{ap,BC}(365)$ based on PSAP measurements and an AAE_{BC} of 1 versus total PSAP absorption at 365 nm, we obtained a slope of 0.81 ± 0.09 and an intercept of −0.74 ± 3.29 (Figure S5). A slope near 1 and a relatively good correlation ($r = 0.91$) indicate a reasonable closure between extract-derived

BrC plus PSAP-derived BC and PSAP absorption for the agricultural fire plumes, although there are uncertainties associated with the assumptions made. *Forrister et al.* [2015] determined from liquid extracts a similar fresh $\Delta b_{ap,BrC}(365)/\Delta CO$ of 0.25 Mm^{-1} $ppbv^{-1}$ in the very large plume of the Rim Fire. In this study, the relatively good correlation ($r^2 = 0.53$) between $\Delta b_{ap,BrC}(365)/(\Delta CO + \Delta CO_2)$, analogous to EFs but in a unit of Mm^{-1} ppb^{-1}, and MCE indicates that BrC was mainly a product of smoldering combustion.

3.2. Plume Evolution

Among the 15 agricultural fires, 13 included at least one long-axis penetration providing samples of both the fresh and aged plume (Table 2). To study the evolution of reactive species, we selected all seven fires that provided aged samples older than 20 min: Fires 1, 3, 4, 12, 13, 14, and 15. As discussed in section 2.3, the downwind changes discussed here were driven mainly by chemical and physical evolution rather than source changes. However, since the $\Delta BC/\Delta CO$ exhibited an increasing trend for Fire 12 (Figure S3), it is possible that the downwind evolution of the species in this fire discussed here reflected both source changes to some extent and plume aging.

When using downwind NEMRs to illustrate evolution, we plot all available data for a single fire together to show the general trend even if these data were from multiple penetrations through the fire. The 1σ uncertainty in the estimated age is based on the variability of wind direction and wind speed. Absolute uncertainties of NEMRs are a result of error propagation from measurement uncertainties. The uncertainties of estimated age and NEMRs (or ERs) are only shown for one fresh and one aged measurement for each fire as examples. Linear or polynomial fits were performed to the NEMRs versus smoke age plot as a simple representation of the evolution trend and also an estimation of the final NEMR at the age of the last measurement. The species we focus on include O_3, reactive nitrogen species, OA, and BrC.

3.2.1. Ozone

In Figure 5, $\Delta O_3/\Delta CO$ for the seven aged fires is plotted versus the estimated smoke age. The initial $\Delta O_3/\Delta CO$ is sometimes negative because the background O_3 can be depleted by fast reaction with freshly emitted NO. Negative initial $\Delta O_3/\Delta CO$ has been frequently observed in fresh BB plumes [*Yokelson et al.*, 2003; *Akagi et al.*, 2012]. In general, rapid O_3 formation was observed in six out of seven agricultural fires. The only exception is Fire 3, in which the less-intense ultraviolet light in late afternoon likely retarded the photochemistry (local flight times are shown in Table 2). $\Delta O_3/\Delta CO$ for the other six fires increased from near zero to 0.03–0.05 in ~30 min after emission. For Fires 4, 14, and 15, the ratio reached over 0.10 or more in about 1 h. Such a formation rate is comparable to that observed in prescribed fires in South Carolina [*Akagi et al.*, 2013] and tropical BB plumes as reviewed in *Akagi et al.* [2011] and faster than those observed in some midlatitude and high-latitude BB plumes [*Goode et al.*, 2000; *Alvarado et al.*, 2010; *Akagi et al.*, 2012].

3.2.2. Reactive Nitrogen Species

NO_x emitted from BB can be converted to HNO_3, nitrate, peroxyacyl nitrates (PANs), alkyl nitrates, and other peroxy nitrates. Figure 6 shows the evolution of excess NO, NO_2, PAN, HNO_3, and nitrate normalized by measured excess NO_y for the selected seven fires. These species constituted ~0.82–0.96 of the total measured NO_y. This fraction did not show significant evolution during aging when compared to combined measurement uncertainty. Several organic nitrates produced by the first and second generation isoprene oxidation such as isoprene hydroxynitrates and MVK/MACR nitrates were also measured at high frequency but no significant elevation or evolution was seen in the plumes. Although not discussed in this section, their observations will be used to evaluate model performance in section 3.3. Other reactive nitrogen species were either not measured (such as HONO) or were measured at a lower time resolution so that such an evolution analysis is limited.

Immediately after emission, NO_x constituted 0.69–0.82 of the total reactive nitrogen (NO_y). The $\Delta NO_x/\Delta NO_y$ ratios decreased with smoke age. Similar to the trend of $\Delta O_3/\Delta CO$, the conversion of NO_x to other reactive nitrogen species was slow in the late afternoon smoke plume of Fire 3. The decrease of $\Delta NO_x/\Delta NO_y$ was much faster in the other five fires in which NO_x measurements were available. In these five plumes, NO_x loss ranged from ~26% to ~56% in about 30 min.

Figure 6 also shows the growth in $\Delta PAN/\Delta NO_y$. For all of the cases but Fire 3, the $\Delta PAN/\Delta NO_y$ ratios increased rapidly from less than 0.05 to ~0.3 in ~1 h. Such a PAN formation rate is similar to that observed in a boreal smoke plume (Lake McKay) during the Arctic Research of the Composition of the Troposphere from Aircraft and Satellites (ARCTAS-B) campaign [*Alvarado et al.*, 2010] and higher than in a Yucatan BB plume [*Yokelson et al.*, 2009] and in the chaparral fire in California [*Akagi et al.*, 2012]. Based on the increase in $\Delta PAN/\Delta NO_y$,

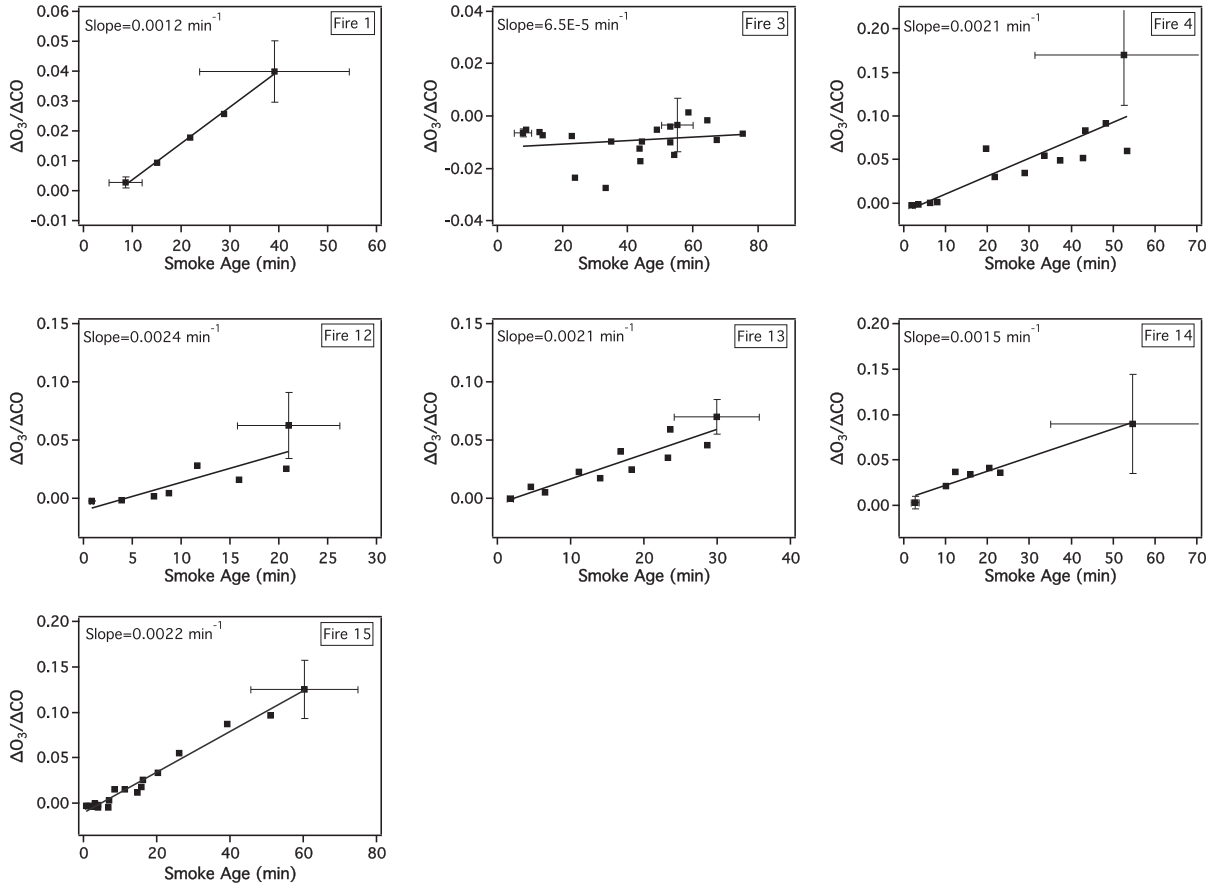

Figure 5. Evolution of ozone in the seven aged plumes. Data were fit to a linear trend line. Vertical error bars are a result of measurement uncertainties. Only error bars of one fresh and one aged measurement are shown as examples for each fire. Horizontal error bars represent the 1σ uncertainty in the estimated age based on the variability of wind direction and wind speed. Note that the downwind evolution of Fire 12 might reflect both source changes to some extent and plume aging.

PAN accounted for 51% to 74% of the loss of NO_x on a molar basis at the end of our aging measurements on each fire. No significant increasing trend was observed for HNO_3. As the plumes aged, HNO_3 concentrations in general remained near background level. Although NH_3 was not measured in this campaign, significant amounts of NH_3 have been observed in other BB studies (Table 5), including crop residue burning [*Akagi et al*., 2011; *Stockwell et al*., 2014]. For example, *Stockwell et al*. [2014] measured an NH_3 EF of Asian rice straw as high as 1.12 ± 0.77 g/kg, adjusted to the SEAC^{4}RS-averaged MCE. Therefore, HNO_3 formed from NO_2 oxidation might have been converted efficiently to nitrate due to the availability of NH_3 and aerosol surface area in the plumes. The trend in Δnitrate/ΔNO_y is most similar to that of ΔPAN/ΔNO_y, suggesting a rapid formation of nitrate particles in the first hour of aging. For the fires including Fires 1, 3, 4, 12, and 14, while ΔPAN/ΔNO_y and Δnitrate/ΔNO_y increased at slightly different rates, the excess PAN and nitrate of the last few measurements accounted for roughly the same fraction of the excess NO_y. This suggests that during the ~1 h aging, approximately equal amounts of initial NO_x emissions were converted to PAN and to nitrate. For Fires 13 and 15, a larger fraction of NO_x was converted to nitrate than to PAN, with nitrate dominating the downwind NO_y budget. Our 1 h Δnitrate/ΔPAN ratios equal to or slightly larger than 1 are the largest values reported to date. On a time scale of several hours, *Akagi et al*. [2012] and *Alvarado et al*. [2010] both observed an average Δnitrate/ΔPAN ratio of ~0.5 in the chaparral fire in California and in boreal forest fire plumes in Canada, respectively. It is also possible that PAN formation becomes increasingly dominant over HNO_3/nitrate formation further downwind, as simulated by *Mason et al*. [2001], so that our Δnitrate/ΔPAN ratio may decrease as the plumes get older than 1 h. PAN and nitrate together accounted for almost all NO_x loss, ranging from 100% to 140% if based on Δnitrate/ΔPAN, ΔPAN/ΔNO_y, and $\Delta NO_x/\Delta NO_y$ ratios. However, such an estimate is uncertain since ΔNO_y is not a strictly conserved tracer in plumes. We will further discuss the conversion of NO_x to PAN and HNO_3/nitrate and the branching between them in section 3.3 using our model simulations.

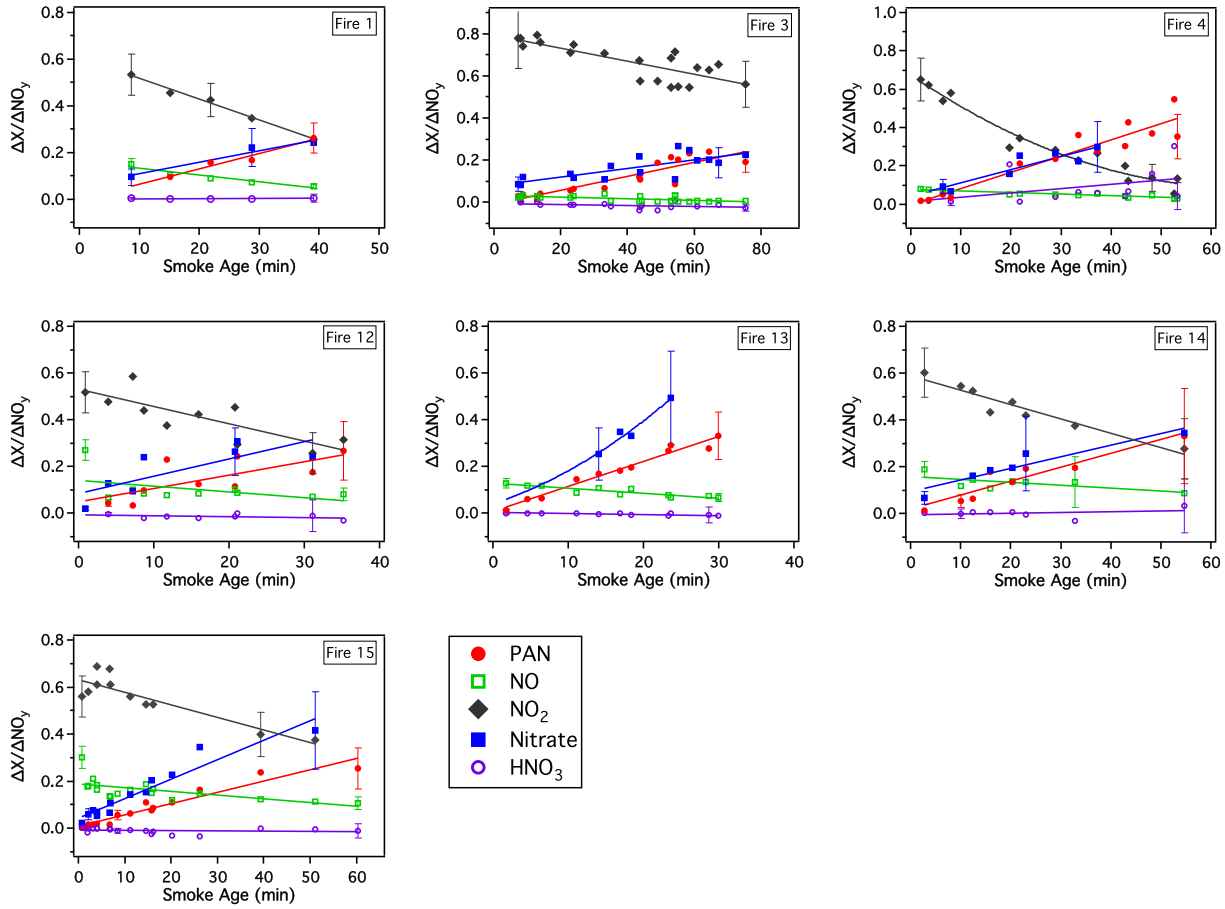

Figure 6. Evolution of reactive nitrogen species in the seven aged plumes. Data were fit to a linear or polynomial trend line. Vertical error bars are a result of measurement uncertainties. Only error bars of one fresh and one aged measurement are shown as examples for each fire. The 1σ uncertainty in the estimated age is same as that shown in Figure 5. NO_2 measurements are not available for Fire 13. Note that the downwind evolution of Fire 12 might reflect both source changes to some extent and plume aging.

3.2.3. Organic Aerosol and Brown Carbon

The changes in ΔOA/ΔCO were also measured for the seven aged fires and were found to vary from fire to fire. The net formation of SOA may contribute to higher downwind ΔOA/ΔCO, while the net evaporation of semivolatile OA may decrease OA mass during dilution and thus reduce ΔOA/ΔCO. The ratio may also stay approximately constant despite active oxidation chemistry, if the different processes approximately cancel in terms of their changes of OA mass [*Cubison et al.*, 2011]. For Fires 12, 13, and 15 sampled on 23 September a possible net increase in ΔOA/ΔCO might have been present (Figure S6). However, no significant increase was seen for the other fires. To represent the overall ΔOA/ΔCO evolution, the changes in ΔOA/ΔCO for all the seven fires were compiled in a single box and whisker plot (25th–75th and 10th–90th percentiles), as shown in Figure 7a. Within the first 15 min, the median $[\Delta OA/\Delta CO]_t/[\Delta OA/\Delta CO]_0$ is 0.96. In downwind plumes the median $[\Delta OA/\Delta CO]_t/[\Delta OA/\Delta CO]_0$ varies between 0.85 and 1.3 and is not significantly different from 1 or the freshest $[\Delta OA/\Delta CO]_t/[\Delta OA/\Delta CO]_0$. The fact that no significant change in the study-averaged ΔOA/ΔCO was observed for the first ~1.2 h aging does not permit strong conclusions about consistent SOA formation in the plumes. *Capes et al.* [2008], *Cubison et al.* [2011], *Hecobian et al.* [2011], *Akagi et al.* [2012], *Jolleys et al.* [2012], and *Forrister et al.* [2015] also observed nearly constant ΔOA/ΔCO with changes smaller than ~20% during aging in open BB plumes. In contrast, within a fire plume over the Yucatan, *Yokelson et al.* [2009] observed a significant enhancement in ΔOA/ΔCO with a growth factor of 2.3 ± 0.85 at 1.4 h of aging. For 60 BB plumes in South Africa, *Vakkari et al.* [2014] observed that aged daytime ΔOA/ΔCO was 4 times that of unprocessed nighttime ΔOA/ΔCO. Laboratory experiments have reported OA enhancement ratios between 0.75 and 3 as a result of photochemical oxidation after a few hours to a few days of exposure to

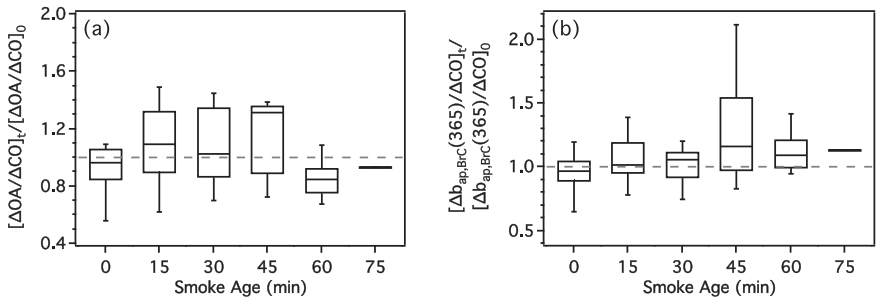

Figure 7. Box and whisker plot of (a) ΔOA/ΔCO change and (b) $\Delta b_{ap,BrC}(365)/\Delta CO$ change in the seven aged plumes (boxes, 25th and 75th percentiles; whiskers, 10th and 90th percentiles; solid horizontal lines, medians; and the two thick lines mean that only one data point is available for the corresponding age). Dashed horizontal lines represent a constant value of 1, i.e., no enhancement.

typical atmospheric OH levels [*Grieshop et al*., 2009; *Hennigan et al*., 2011; *Ortega et al*., 2013]. The reasons for the observed variability in net SOA formation from BB plumes are not well understood.

To investigate the chemical transformations of OA, we analyzed elemental ratios including oxygen-to-carbon (O/C) and hydrogen-to-carbon (H/C) ratios using data from the aerosol mass spectrometer (AMS) [*Aiken et al*., 2008; *Canagaratna et al*., 2015]. Figure 8 shows the evolution of these two elemental ratios and also background ratio values for six fires. Elemental ratios for Fire 12 were not available. The measurement uncertainties of O/C and H/C are 28% and 13%, respectively, based on *Canagaratna et al*. [2015]. The background H/C ratios were in the range of 1.5–1.7 and were always smaller than the H/C ratio near the burning sources, which were generally between 1.6 and 1.8. In contrast, the background O/C ratios (0.7–0.9) were higher than the O/C ratios for POA from the agricultural fires (0.3–0.5), which are similar to the values observed in BB plumes over the Mexico City basin [*DeCarlo et al*., 2008]. Lower O/C and higher H/C values than background values suggest that POA produced by crop residue burning contained more reduced and less oxidized compounds than background OA. For all six plumes, a consistent increase in the O/C ratios and a decrease in the H/C ratios associated with aerosol aging were observed, although at different rates. Processes that could explain the observed elemental ratio trends include (1) mixing with background OA, (2) chemical processing, and (3) the preferential evaporation of more reduced species. Although mixing with background OA would eventually increase O/C and decrease H/C toward the background values, this is likely not the dominant effect. For five out of the six cases, O/C ratios increased from around ~0.4 to 0.6–0.8 in less than 1 h. Since the measurements indicated that the excess OA concentrations in plumes were well beyond the background OA concentrations throughout this period, mixing alone could not have contributed enough background OA to account for such a rapid O/C increase (Figure 12b, as will be discussed in section 3.3.4). When combined with the approximately constant $[\Delta OA/\Delta CO]_t/[\Delta OA/\Delta CO]_0$ ratios, the observations in O/C and H/C ratios show that the addition of oxygen must be offset by the loss of carbon during aging so that both chemical processing and evaporation were contributing. Rapid O_3 formation also serves as evidence of photochemical activity within the plumes. Chemical processing could change elemental ratios by the addition of SOA of higher O/C ratios or the heterogeneous oxidation of POA. Not surprisingly, the changes of O/C and H/C ratios were slowest in the plume of Fire 3, which agrees with the overall slow photochemistry. This provides further evidence that, in general, SOA formation was active on this time scale and that not all the O/C changes can be explained by differential evaporation.

BrC in POA and SOA in BB plumes may also evolve. The aging effects on the light-absorbing properties of organic carbon vary among studies perhaps due to different aging times and oxidation conditions [*Adler et al*., 2011; *Saleh et al*., 2013; *Zhong and Jang*, 2014; *Forrister et al*., 2015]. To investigate the influence of aging on short-wavelength light absorption, we plotted box and whisker plot of the changes in $\Delta b_{ap,BrC}(365)/\Delta CO$ for the seven fires (Figure 7b). Similar to Figure 7a, $[\Delta b_{ap,BrC}(365)/\Delta CO]_t/[\Delta b_{ap,BrC}(365)/\Delta CO]_0$ was used to represent $\Delta b_{ap,BrC}(365)$ evolution. In Figure 7b, the downwind $[\Delta b_{ap,BrC}(365)/\Delta CO]_t/[\Delta b_{ap,BrC}(365)/\Delta CO]_0$ exhibits slightly higher median values and upper limits than the fresher samples less than 15 min old. The slight increase in $\Delta b_{ap,BrC}(365))/\Delta CO$ suggests that the aged aerosols up to ~1.2 h old were more absorptive than fresh OA. This could possibly result from SOA formation, as implied by the O/C increase. Other processes

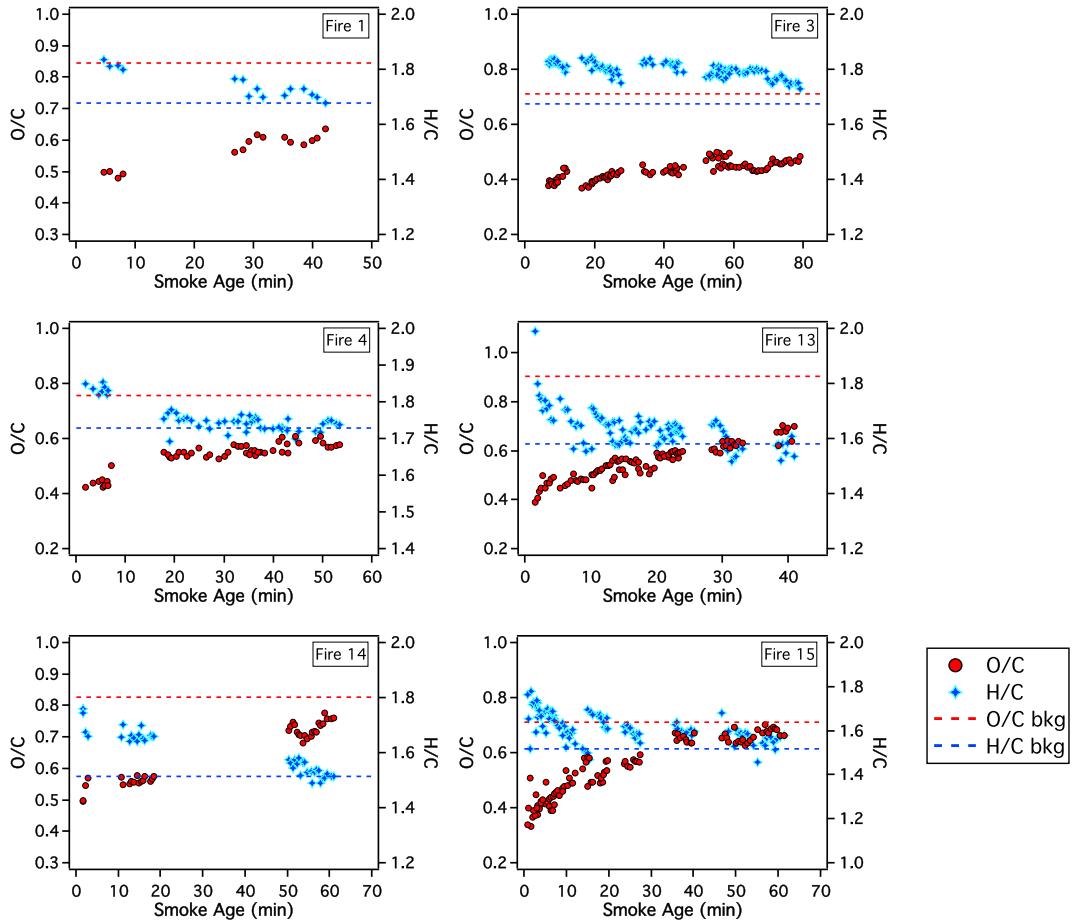

Figure 8. Evolution of elemental ratios in particulate matter as measured by the AMS in six aged plumes (not available for Fire 12).

could also be occurring, such as the loss of volatile BrC and photobleaching. On a similar time scale, *Saleh et al*. [2013] also reported that aged OC was more absorptive due to SOA formation in a smog chamber experiment. *Zhong and Jang* [2014] reported that chromophore formation and sunlight bleaching governed the change in the absorption of wood smoke aerosol. During a diurnal cycle, OA absorption was first enhanced by chromophore formation in the morning and then decreased by sunlight bleaching in the afternoon. On a longer time scale, *Forrister et al*. [2015] demonstrated that BrC emitted from wildfires was largely unstable and decayed in the plume with a half-life of 9 to 15 h. Therefore, our measurements in agricultural fire plumes may have captured BrC evolution in the early stage before its loss exceeded possible secondary formation.

3.3. Model Simulations

Understanding the rapid chemical evolution in fire plumes is critical for evaluating the impact of agricultural fires on regional air quality, atmospheric composition, and climate. Here we use the LPCS-REAM model to simulate the evolution of O_3, PAN, HNO_3, nitrate, radicals, SOA, and the O/C ratios within young agricultural fire plumes.

Figure 9 shows the simulated CO mixing ratios using the best fit dilution coefficient (K_y), one half of best fit K_y, and twice of best fit K_y, along with the observed CO mixing ratios. Despite the assumptions made for a single K_y value and the method of observation-model comparison, the simulated CO mixing ratios using the best fit K_y reasonably represented the dilution trend when compared to the observations. The overall successful agreement enables us to further study the chemical evolution in the fire plumes.

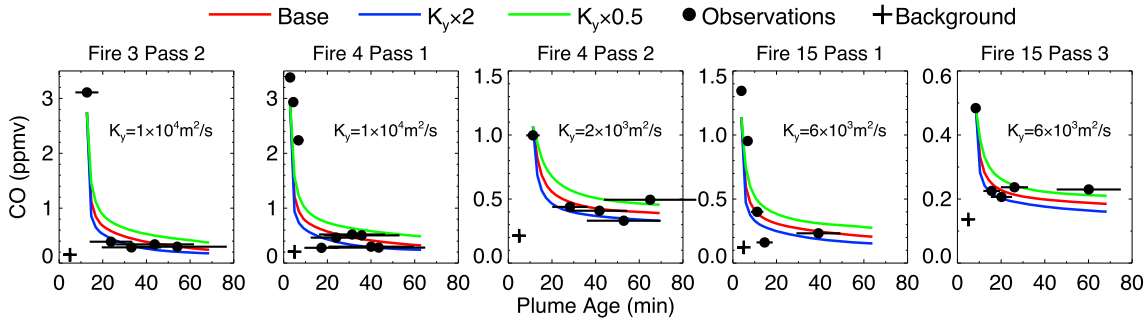

Figure 9. CO mixing ratio versus smoke age for the five selected cases. Green, red, and blue lines are for the slow, best fit, and fast plume dilution rates. Circles are the measured mixing ratios, with the horizontal error bars showing the uncertainty in the estimated age. Crosses are background CO concentrations outside the plumes.

3.3.1. Ozone

Figure 10 shows the evolution of the enhancement ratios of O_3 for the five selected cases. With the best fit dilution coefficients, the model can reasonably simulate $\Delta O_3/\Delta CO$ to within ~30% in general. To quantify the photochemical O_3 production in an agricultural fire plume, we used the simulated results to calculate ozone production efficiency (OPE), defined as the number of O_3 molecules produced per number of NO_x molecules oxidized [*Liu et al.*, 1987; *Lin et al.*, 1988; *Trainer et al.*, 1993; *Olszyna et al.*, 1994]. In this study, we computed the OPEs during 1 h evolution by dividing the number of O_3 molecules produced by the number of NO_x molecules oxidized to PAN and HNO_3 + nitrate, given that PAN and HNO_3 + nitrate accounted for most of the measured NO_x oxidation products (Figure 6). As shown in Table 6, the OPEs are in a range of 6.0 to 9.8 for the five cases. OPE values on the time scales of 0.5–4 days were estimated to be 5–17 for BB activities in Southeast Asia [*Kondo et al.*, 2004], South and Central Africa [*Marion et al.*, 2001; *Yokelson et al.*, 2003], Australia [*Shirai et al.*, 2003; *Takegawa et al.*, 2003], and western U.S. [*Baylon et al.*, 2015]. The OPEs for the agricultural fires are in the lower end of the previously reported range. However, the OPEs in our cases will likely evolve as age increases beyond 1 h. The thermal decomposition of PAN could also further promote O_3 production after the first 1 h.

3.3.2. Reactive Nitrogen Species

The simulated enhancement ratios of the major NO_x oxidation products, PAN, HNO_3, and nitrate, are shown in Figure 11. Note that the nitrate observations shown are the total nitrate measured by AMS, while the modeled nitrate represents the sum of initial emissions plus those originating from HNO_3 condensation. As the AMS measurements indicated that the nitrate in all the fire plumes in this study was mainly composed of inorganic nitrate (>90%), comparing the evolution of measured total nitrate with that of the modeled inorganic nitrate is reasonable. Table 6 shows the ratio between NO_x oxidized to PAN and that oxidized to PAN plus HNO_3 + nitrate. It can be seen from Figure 11a that the model, in general, underestimated the formation of PAN by up to ~50% of the observed $\Delta PAN/\Delta CO$. The simulated HNO_3 was generally lower than the observed HNO_3 as the simulated $\Delta HNO_3/\Delta CO$ decreased more rapidly with age than the observations (Figure 11b). For

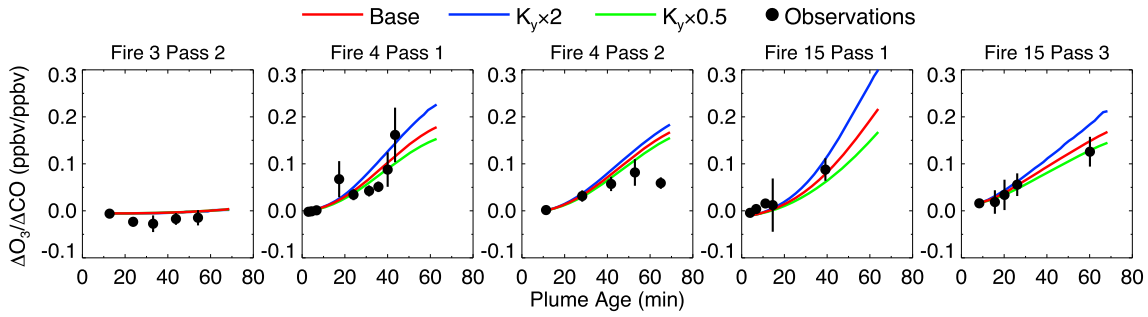

Figure 10. Enhancement ratios of ΔO_3 to ΔCO versus smoke age for the five selected cases. Green, red, and blue lines are for the slow, best fit, and fast plume dilution rates. Circles are the measured enhancement ratios, with the vertical error bars showing the uncertainty in the measurement. The uncertainty in the estimated age is not shown here but is same as in Figure 9.

Table 6. Summary of the Modeled Evolution Characteristics at an Age of 1 h: Ozone Production Efficiency (OPE), the Ratio of NO_x Oxidized to PAN to That Oxidized to PAN Plus HNO_3 + Nitrate (P_PAN/(P_HNO_3 + P_PAN)), and Radical Concentrations

Case	OPE	P_PAN/(P_HNO_3 + P_PAN)	OH (molecules cm^{-3})		HO_2 (molecules cm^{-3})		RO_2 (molecules cm^{-3})	
			Median	Average	Median	Average	Median	Average
Fire 3 Pass 2	6.0	0.65	5.6×10^5	5.3×10^5	1.5×10^8	1.4×10^8	6.7×10^7	6.6×10^7
Fire 4 Pass 1	7.0	0.66	1.7×10^7	1.5×10^7	1.2×10^9	1.1×10^9	3.8×10^8	4.1×10^8
Fire 4 Pass 2	9.8	0.50	1.9×10^7	1.8×10^7	1.0×10^9	1.0×10^9	2.8×10^8	2.9×10^8
Fire 15 Pass 1	6.3	0.39	1.5×10^7	1.7×10^7	2.5×10^8	3.3×10^8	8.9×10^7	1.1×10^8
Fire 15 Pass 3	7.2	0.62	7.5×10^6	6.7×10^6	3.9×10^8	3.5×10^8	1.4×10^8	1.3×10^8

nitrate, the model performance varied from case to case. For Fire 3 Pass 2 and Fire 4 Passes 1 and 2 (Figure 11c), the increase of Δnitrate/ΔCO was overestimated by the model by up to ~50%. In these three cases, the underestimation of HNO_3 and the overestimation of nitrate imply that the model exaggerated the gas-to-particle deposition of HNO_3. In the other two cases, Fire 15 Passes 1 and 3, the model underestimated nitrate, although within measurement uncertainties. However, more downwind nitrate data are needed for better evaluation. Since modeling the partitioning between HNO_3 and nitrate is limited by the simplified treatment of HNO_3 deposition, it is also useful to compare the observed and the simulated sum of HNO_3 + nitrate. As also shown in Figure 11b, the model made reasonable predictions for total HNO_3 + nitrate for the first three cases within measurement uncertainties but underestimated the concentrations of total HNO_3 + nitrate for the last two cases,

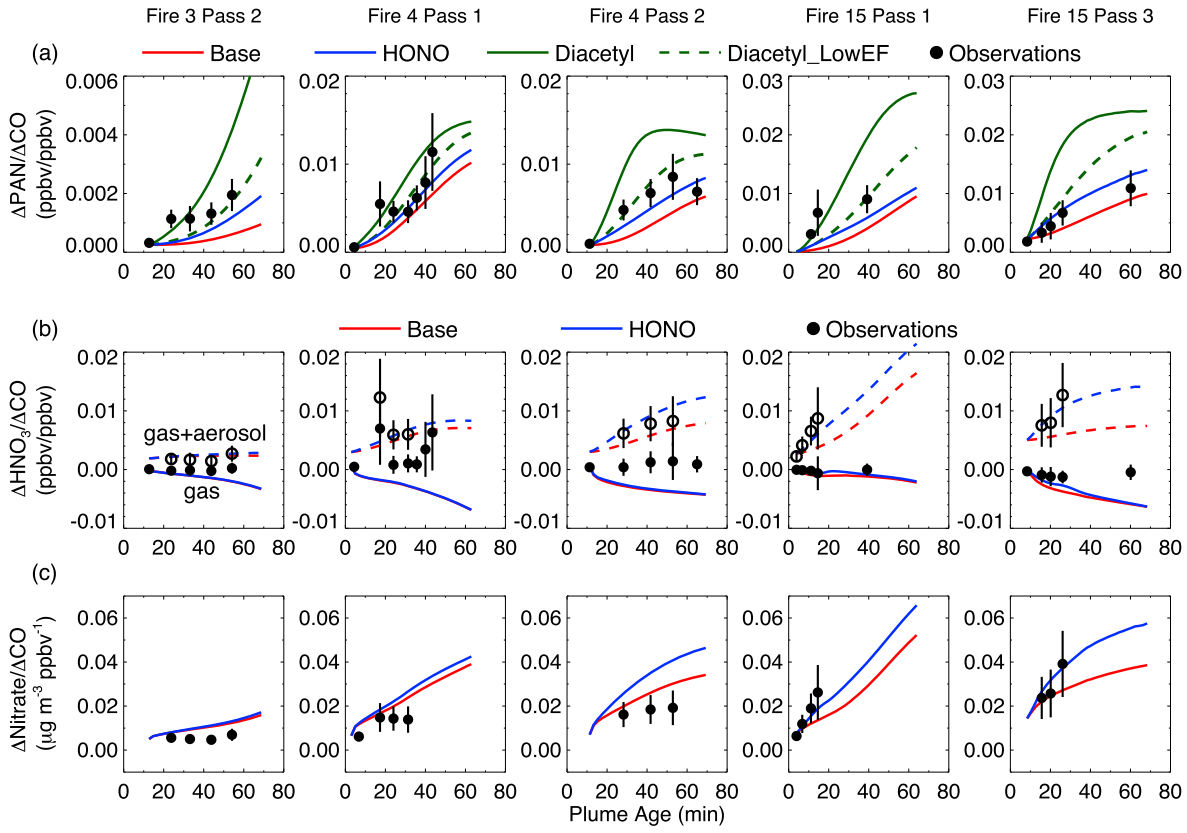

Figure 11. Enhancement ratios of (a) ΔPAN to ΔCO, (b) ΔHNO_3 to ΔCO and (ΔHNO_3 + Δnitrate) to ΔCO, and (c) Δnitrate to ΔCO versus smoke age for the five selected cases. Circles (solid circles for single NO_y species and open circles for HNO_3 by CIMS + nitrate by AMS) are the measured enhancement ratios, with the vertical error bars showing the uncertainty in the measurement. The uncertainty in the estimated age is not shown here but is same as in Figure 9. The red lines (solid and dashed) are base model results for the best fit dilution rates. The blue (solid) and green (solid and dashed) lines are the results of the base model with estimated HONO (using FLAME-4 EF) and diacetyl (using FLAME-4 EF and one half of FLAME-4 EF) initial emissions.

although again more downwind nitrate data would be useful to better evaluate the model performance. Several reasons may explain the disagreement. First, the highest initial emissions of nitrate near the fire sources were not measured for the Fire 3 Pass 2 and Fire 4 Pass 1. The input of the freshly emitted nitrate was estimated using the EF(nitrate) from other transects of the same fire and measured CO peak, which is a source of uncertainty for downwind nitrate simulation. Second, errors in the modeled photochemistry, e.g., the modeled OH concentration, could bias the HNO_3 + nitrate predictions.

The model output also includes other gaseous organic nitrate, including peroxypropionyl nitrate (PPN), peroxymetacryloyl nitrate, NO_3CH_2PAN, isoprene organic nitrates, carbonyl nitrates from NO_3 + isoprene, methyl nitrate, and C_4- and C_5-alkyl nitrates. According to the simulation, the sum of these gaseous organic nitrates was elevated by 0.1–0.3 ppbv at an age of 1 h after accounting for dilution, which is minor compared to PAN or HNO_3 + nitrate formation. The available fast measurements of PPN and several organic nitrates produced from isoprene oxidation showed that their formation was of similar magnitude as predicted by the model. In addition, the organic nitrate fractions for all the fires in this study reported by the AMS were $<$10%, which indicates that the enhancement of particulate organic nitrate was smaller than or similar to that of gaseous organic nitrates. So it is likely that only a small amount of gaseous organic nitrates that formed, if any, partitioned to the particle phase.

Several sensitivity simulations were performed to explore possible reasons for the underestimation of PAN (all five cases) and HNO_3 + nitrate (the last two cases) formation (Figure 11). Since the VOCs measured at sampling rates $\geq$ 10 s (Table 1) likely missed the highest peak near fire sources and thus underestimated the initial emissions from the fires, additional model runs were performed with enhanced VOC initial concentrations. The results indicate that as expected, acetaldehyde had the most significant influence on PAN formation. However, doubling the acetaldehyde concentration still cannot fully explain the observed rapid formation of PAN (Figure S7). Simulations were conducted with additional unmeasured species, including HONO, methylglyoxal, diacetyl, and MEK. Their initial emissions were scaled using FLAME-4 EFs (adjusted to SEAC^{4}RS MCE) and measured CO initial emissions [*Stockwell et al*., 2015]. The results showed that, with EFs from FLAME-4, HONO (0.35 ± 0.13 g/kg) and diacetyl (0.92 ± 1.00 g/kg) were significant contributors to PAN formation (Figure 11a), while methylglyoxal (0.36 ± 0.31 g/kg) was relatively less important (Figure S7). A combined effect of adding HONO, diacetyl, and methylglyoxal is shown in Figure S7. Since PAN was very sensitive to diacetyl, the large variability of EF(diacetyl) could lead to a large uncertainty in the simulated PAN. We found that by reducing EF(diacetyl) by a factor of 2, the simulated ΔPAN/ΔCO agreed well with the observed values (Figure 11a). The addition of initial HONO also promoted the modeled HNO_3 + nitrate formation by ~30–70% and resulted in better agreements with observations especially for the last two cases (Figure 11b). This suggests that the baseline simulation is likely missing some radical sources. The measured acetaldehyde, methylglyoxal, and diacetyl were also found to be the main precursors of peroxyacetyl radicals in the plume of the small forest understory fire in Georgia reported by *Müller et al*. [2016].

3.3.3. Radical Concentrations

BB greatly perturbs atmospheric oxidants. For example, the direct emissions and the secondary formation of hydrogen peroxide, formaldehyde, and other aldehydes from BB can be significant sources of hydrogen oxides (HO_x) [*Lee et al*., 1998; *Trentmann and Andreae*, 2003; *Yokelson et al*., 2009; *Müller et al*., 2016]. In addition, the oxidation of emitted organic species produces organic peroxy radicals (RO_2), which can propagate HO_x and NO_x radical chains and thereby generate O_3 through subsequent photolysis of NO_2 [*Orlando and Tyndall*, 2012]. Although measurements of HO_x or RO_2 were not available, we present model estimates to characterize the oxidants within the agricultural fire plumes. Table 6 lists the median and average concentrations of OH, hydroperoxyl radical (HO_2), and RO_2 during the 1 h simulation. For Fire 3 Pass 2, the low modeled radical concentrations agree with the overall slow photochemistry. For the other four cases, the average OH and HO_2 concentrations were in the ranges of 6.7×10^6 to 1.8×10^7 molecules cm^{-3} and 3.3×10^8 to 1.1×10^9 molecules cm^{-3}, respectively. The photochemical production of the HO_x family in the plume was dominated by the photolysis of formaldehyde and the reaction of $O^1D + H_2O$ (from O_3 photolysis), which on average accounted for ~60% and ~35%, respectively. As a comparison, *Hobbs et al*. [2003] inferred an average OH concentration of $\sim 1.7 \times 10^7$ molecules cm^{-3} from the relative rates of decrease for a number of chemical species in a savanna fire plume burned in South Africa in late morning. *Yokelson et al*. [2009] measured a similar OH level of 1.14×10^7 molecules cm^{-3} from a slightly aged plume that was 22–43 min old. Without being influenced by BB, the average noontime OH and HO_2 concentrations at the surface in

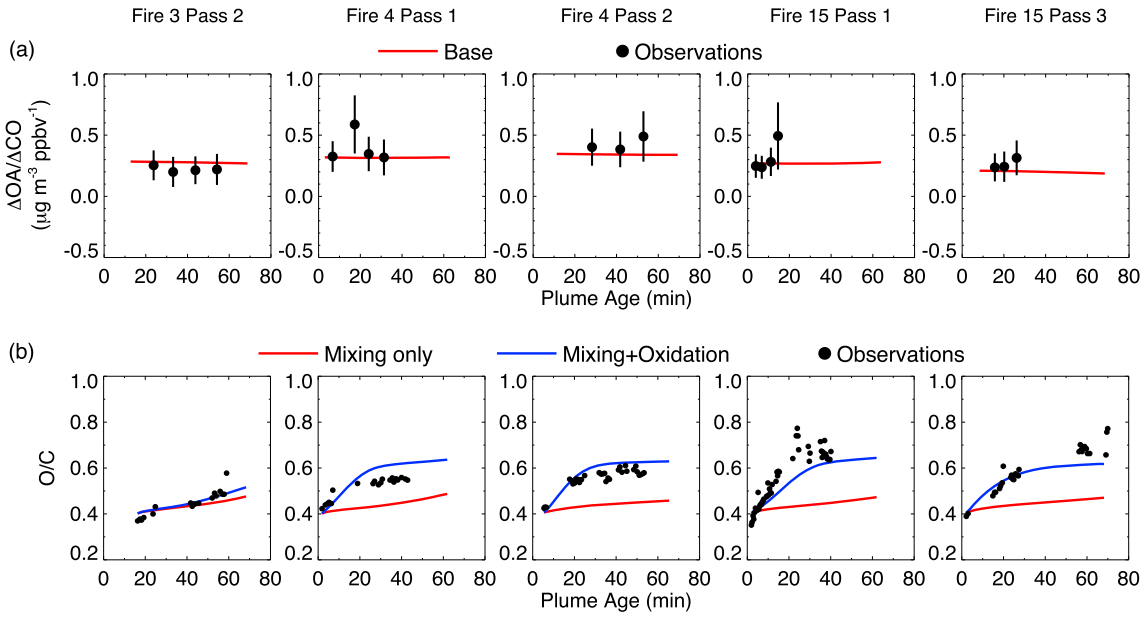

Figure 12. (a) Enhancement ratios of ΔOA to ΔCO versus smoke age for the five selected cases. Circles are the measured enhancement ratios, with the vertical error bars showing the uncertainty in the measurement. The uncertainty in the estimated age is not shown but is same as in Figure 9. The red lines are parameterization results for the best fit dilution rates assuming OA is nonvolatile. (b) Elemental O/C ratios versus smoke age for the five selected cases. Dots are the measured O/C ratios. The red and blue lines are model results of mixing effects only and of both mixing and oxidation effects, respectively.

the southeastern U.S. measured in summer 2013 were ~2.4×10^6 (0.1 ppt) and ~1.2×10^9 molecules cm^{-3}, respectively [*Xiong et al.*, 2015]. In short, the photochemical environment in the plumes studied here has similar levels of OH as those in *Hobbs et al.* [2003] and *Yokelson et al.* [2009] and generally higher OH, up to ~8 times higher, than the surface ambient air studied in *Xiong et al.* [2015]. The magnitude of simulated HO_2 in the plumes is similar to that in *Xiong et al.* [2015]. In the case of RO_2, the average modeled concentration ranged from 6.6×10^7 to 4.1×10^8 molecules cm^{-3}, with methyl peroxy radical (CH_3O_2) accounting for ~30–50% of RO_2. As discussed before, the radical concentrations reported here likely represent a lower limit on actual radical levels in the agricultural fire plumes.

3.3.4. SOA and O/C Ratios

SOA formation in the plumes was calculated by a simplified parameterization, which was proposed based on urban pollution observations made in Mexico City [*Hodzic and Jimenez*, 2011] and Los Angeles [*Hayes et al.*, 2015], with parameters updated for biomass burning emissions based on *Cubison et al.* [2011]. Figure 12a shows the modeled ΔOA/ΔCO versus plume age for the five individual passes. The simulated ΔOA/ΔCO is the sum of the observed POA/ΔCO and the modeled SOA/ΔCO, where POA is treated as nonvolatile during the ~1 h aging considered here. The model parameters ensured that ΔOA/ΔCO was generally conserved for all the five cases after considering dilution, indicating that SOA formed in 1 h was insignificant compared with POA emitted. Although there are discrepancies between the simulations and the observations, several factors limit a detailed parameter optimization. First, for Fire 3 Pass 2, Fire 4 Pass 1, and Fire 15 Pass 3 in Figure 12a, POA emissions were not measured but were estimated from the EF(OA)s of the corresponding fires obtained from other transects, which may contribute to downwind discrepancies between modeled and observed ΔOA/ΔCO. Second, the short aging time and the limited number of downwind samples also make it less meaningful for a detailed parameter optimization. In our simulation, the EF of 0.013 g of the lumped SOA precursor per gram of CO worked well for the agricultural fires, although a lower EF could have also worked due to the insignificant SOA formation observed. Since the ratio of the average EF for the VOCs listed in Table 3 to that of CO is already as high as 0.16 g g^{-1}, this implies a net SOA yield of the order of 10%.

The evolution of the O/C ratio due to oxidation was also empirically estimated using equation (7). Note that since POA accounted for the majority of the mass of OA in the plumes, equation (7) can be regarded as a parameterization for the O/C increase in the bulk OA, which was composed of POA and some SOA. In Figure 12b, the red lines are the O/C increases due to the mixing effect only and the blue lines represent the sum of

mixing and chemical processing effects, both assuming a POA O/C ratio of 0.4 based on observations. In Fire 3 Pass 2 (Figure 12b), consistent with the low simulated OH, the slow increase of O/C was almost solely due to mixing with background air rather than chemical oxidation. In other cases with sufficient oxidation, our parameterization generally agreed with the observed O/C increases. Although highly uncertain, the photochemical aging time scale of 0.05 days used here (equivalent to OH exposure of 0.6×10^{10} molecules cm^{-3} s) is much smaller than that of 1.5 days (equivalent to OH exposure of 1.94×10^{11} molecules cm^{-3} s) for SOA in Mexico City [*Hodzic and Jimenez*, 2011] and Los Angeles [*Hayes et al*., 2015] conditions. In other BB plumes, O/C aging time scales longer than 0.05 days were observed. For example, ~0.1–0.4 days were observed for forest fire plumes in field studies [*Cubison et al*., 2011; *Forrister et al*., 2015] and ~1.2 days when exposing smoke emitted from burning different types of biomass to OH and O_3 in a flow reactor [*Ortega et al*., 2013]. By comparison, the rate of oxidation of OA in the agricultural fire plumes reported here is substantially faster than those in urban plumes, forest fire plumes, and smoke exposed in a flow reactor.

3.4. Annual Emissions of SO_2, NO_x, and CO From Crop Residue Burning in Southeastern U.S.

The measured EFs were used to estimate the annual emissions of three trace gases, SO_2, NO_x, and CO from agricultural field burning in the four states where the agricultural fires were sampled (Arkansas, Louisiana, Mississippi, and Missouri) and hence to compare with the 2011 National Emissions Inventory (NEI; http://www.epa.gov/ttnchie1/net/2011inventory.html; accessed data in June 2015). Although the lab study by *Stockwell et al*. [2014] found roughly similar emissions from various crop materials including rice straw (generally within a factor of 2–3), it is very likely that the emissions of some species can be more variable across crop type (e.g., Table 5). However, since the field EF data for other crops in the U.S. are not available, the same EFs are assumed for all crops to roughly estimate the annual emissions of trace gases from open burning in the four states. This noncrop-type specific EF assumption for SO_2, NO_x, and CO likely results in an uncertainty of about a factor of 2. Emissions were calculated using the *Seiler and Crutzen* [1980] method of multiplying EF, burned area, fuel loading (mass of biomass per unit area), and combustion completeness (fraction of biomass consumed by fire). The EFs obtained in $SEAC^4RS$ were coupled with fire activity data from three studies based on different methods: *McCarty et al*. [2009] is based on remote sensing and *Melvin* [2012] and *Reid et al*. [2004] rely on government statistics. *McCarty et al*. [2009] estimated the area of crop residue burning using satellite data from 2003 to 2007. *Reid et al*. [2004] reported government statistics for agricultural burning for Arkansas, Louisiana, and Missouri collected in 2002. In Figure 10 of *Melvin* [2012], acre ranges of agricultural and forestry prescribed burning in 2011 were based on state records. We estimated the agricultural burning area for each state by multiplying the average prescribed burning area by 37%, which is the overall percentage of agricultural burning in the southeast region according to Figure 5 of *Melvin* [2012]. In addition, the dry mass of rice straw was taken as 0.58 ± 0.14 kg m^{-2} [*Oanh et al*., 2011] and we assume that 100% of biomass was consumed in burning. Figure 13 compares a set of regional emission estimates based on different fire activity data. The first three bars in the two figures are our estimates. The last red bars are the estimates by the 2011 NEI, in which SO_2, NO_x, and CO emission data are available. The error bars of the estimates based on *Melvin* [2012] represent a range corresponding to the burned area range as reported. Total uncertainties are not explicitly shown, in part because there is not enough information to estimate them quantitatively. The appropriate error would include error propagation from the noncrop-type specific EF data and the estimates of biomass burned.

In Figure 13, the estimated emissions of SO_2, NO_x, and CO vary with the fire activity data used. In general, the estimates based on *McCarty et al*. [2009] are the smallest emissions. Emissions estimated from *Reid et al*. [2004] and *Melvin* [2012] and by the 2011 NEI are generally close, and they differ by less than a factor of 2.5 except for Missouri. The fire activity data are highly uncertain, as indicated in Figure 13. While there could have been some variability in fire activities of different years [*McCarty et al*., 2009; *van der Werf et al*., 2010], it is likely the different methods contributed most to the uncertainties in emissions. Three of the four estimates rank Arkansas as the state with the highest agricultural burning emissions among the studied states. Arkansas and Louisiana are also two of the several states that emitted the highest amounts of CO in the contiguous U.S. according to *McCarty* [2011]. Summing up the four states, the average annual SO_2, NO_x, and CO emissions from agricultural fires were ~2%, ~7%, and ~330% of coal combustion emissions estimated in the 2011 NEI. For NO_x and CO, the agricultural fire emissions were about ~1% and ~9% of mobile sources, respectively. These ratios are estimated to have uncertainties between factors of 2.1 and 2.4 by considering

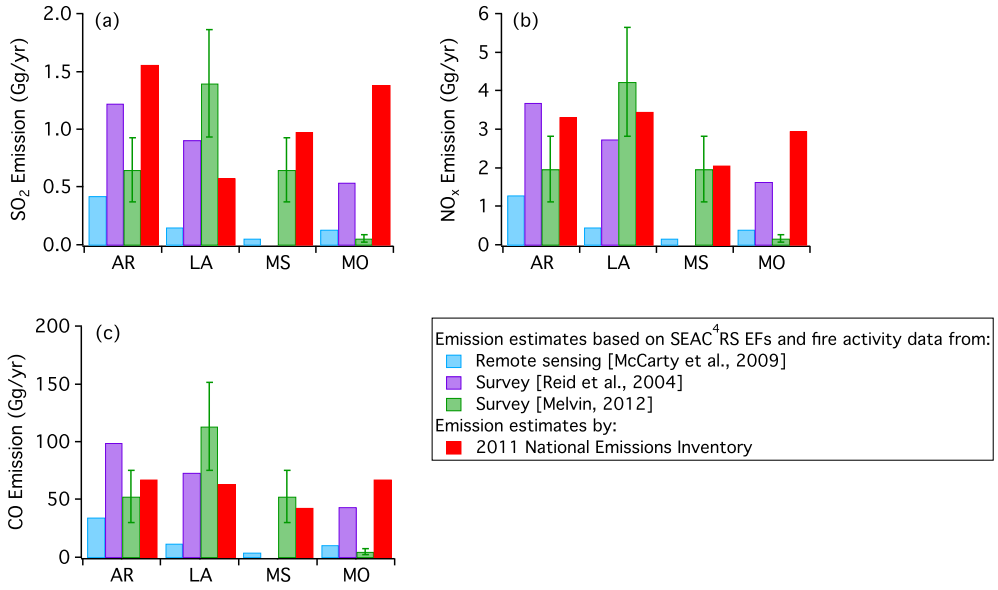

Figure 13. Estimates of annual emissions of (a) SO_2, (b) NO_x, and (c) CO from crop residue burning in Arkansas, Louisiana, Mississippi, and Missouri. NO_x emission estimates are reported as NO_2. The green error bars of the estimates based on *Melvin* [2012] represent the ranges of the burned area reported and are smaller than the overall errors of the emission estimates.

uncertainties in EFs and variations in burned areas. Further investigation is required to obtain realistic burning activities and crop-specific EFs for better emission estimation.

4. Conclusions

The emissions from 15 agricultural fires were measured over the southeastern U.S. from the NASA DC-8 research aircraft. Based on these measurements, this study reports a detailed set of EFs of a number of trace gases and fine particles from agricultural field burning. The aerosol light absorption coefficients measured by PSAP and the light absorption measured from liquid extracts of aerosol implied that BrC was ubiquitous in these fires. The EFs as a function of MCE were examined. Whereas the EFs of VOCs generally showed good anticorrelation with MCE, the EFs of inorganic gases and particles were likely influenced more by fuel composition and fire variability than by MCE and thus had weak correlations with MCE. We also compared the EFs with the limited previous field and lab measurements of crop residue fires. In general, the average EFs of trace gases derived in this work agree well with those reported by *Akagi et al.* [2011], *Hayashi et al.* [2014], *Kudo et al.* [2014], and *Stockwell et al.* [2015]. As for the particle species, the agricultural fires studied here had significantly larger emissions than the lab burning of rice straw [*Hayashi et al.*, 2014].

In addition, 7 out of the 15 fire plumes allowed for a detailed investigation into the chemical evolution of the primary emissions during the first 1.2 h of aging. Rapid enhancement of O_3 was observed with $\Delta O_3/\Delta CO$ reaching ~0.10. Meanwhile, rapid conversion of NO_x to PAN and nitrate was also observed with the ratios of $\Delta PAN/\Delta NO_y$ and $\Delta nitrate/\Delta NO_y$ being generally similar and each reaching up to ~0.4 in about 1 h. Although no significant evolution of OA mass and BrC absorption was seen on average, a consistent increase in O/C elemental ratios associated with aerosol aging indicated that chemical processing was ongoing and that SOA formation consistently occurred but was likely offset by the evaporation of OA. We used the LPCS-REAM model to simulate the chemistry within these young fire plumes. We found that the model reasonably simulated O_3 formation. The formation of PAN was generally underestimated by the model, which implied missing radical sources likely due to unidentified oxygenated compounds or underestimated initial VOC concentrations. Specifically, diacetyl, which is rarely measured in BB, could be a significant contributor to PAN formation. In the case of HNO_3 and nitrate, the model could not fully reproduce their branching. On the other hand, the modeled sums of HNO_3 + nitrate agreed with observations in three cases but were biased low in the other two cases. We speculated that the assumed HNO_3 uptake coefficient or the modeled

photochemistry (e.g., no initial HONO) might be responsible for these discrepancies. As PAN and nitrate accounted for almost all observed NO_x loss, organic nitrates in the gas phase or the particulate phase were not formed efficiently in the agricultural fire plumes. The model also estimated radical concentrations within the fire plumes during the 1 h simulation, with high OH levels that sometimes reached over 1×10^7 molecules cm^{-3}. By implementing the simple empirical parameterization proposed by *Hodzic and Jimenez* [2011] with the parameters of *Cubison et al*. [2011], we modeled the evolution of OA mass. The OA parameterization was generally consistent with the measured OA, although the number of OA samples limited a thorough parameter optimization. After modifying the parameters used in *Hodzic and Jimenez* [2011] to adapt to this study, our O/C parameterization indicated that the aerosol oxidation process within the agricultural fire plumes appeared to be much faster than that in urban atmospheres and forest fire plumes.

With the measured EFs, we also roughly estimated the annual agricultural fire emissions of SO_2, NO_x, and CO from Arkansas, Louisiana, Mississippi, and Missouri. The estimated ratio of the annual primary emissions from agricultural burning to the annual primary emissions from major sources for these species follows: SO_2 (~2% of coal combustion), NO_x (~1% of mobile sources), and CO (~9% of mobile sources). However, these ratios are highly uncertain, about a factor of 2.1–2.4, since the EFs used for crop residues other than rice straw and the burning activity are uncertain. Future investigation of the EFs for different crop fuels, fuel loading, and fire activity will help address the uncertainties in agricultural burning emission inventories.

Acknowledgments

This work was supported by NASA grant NNX12AB77G. R. Yokelson was supported by NASA Earth Science Division Awards NNX12AC20G and NNX14AP45G. PTR-MS measurements during SEAC^{4}RS were supported by the Austrian Federal Ministry for Transport, Innovation and Technology (bmvit) through the Austrian Space Applications Programme (ASAP) of the Austrian Research Promotion Agency (FFG). A.W. and T.M. received support from the Visiting Scientist Program at the National Institute of Aerospace (NIA). P.C. J., D.A.D., and J.L.J. were supported by NNX12AC03G and NNX15AT96G. CIT-CIMS measurements were supported by NASA grants NNX12AC06G and NNX14AP46G-ACCDAM. ISAF HCHO observations were supported by NASA SEAC^{4}RS grant NNH10ZDA001N. The authors would also like to thank the SEAC^{4}RS science team and the DC-8 flight crews. Data from the SEAC^{4}RS mission can be found at http://www-air.larc.nasa.gov/cgi-bin/ArcView/seac4rs and http://www-air.larc.nasa.gov/missions/seac4rs/index.html.

References

Adler, G., J. M. Flores, A. Abo Riziq, S. Borrmann, and Y. Rudich (2011), Chemical, physical, and optical evolution of biomass burning aerosols: A case study, *Atmos. Chem. Phys.*, *11*(4), 1491–1503, doi:10.5194/acp-11-1491-2011.

Aiken, A. C., et al. (2008), O/C and OM/OC ratios of primary, secondary, and ambient organic aerosols with high-resolution time-of-flight aerosol mass spectrometry, *Environ. Sci. Technol.*, *42*(12), 4478–4485, doi:10.1021/es703009q.

Akagi, S. K., R. J. Yokelson, C. Wiedinmyer, M. J. Alvarado, J. S. Reid, T. Karl, J. D. Crounse, and P. O. Wennberg (2011), Emission factors for open and domestic biomass burning for use in atmospheric models, *Atmos. Chem. Phys.*, *11*(9), 4039–4072, doi:10.5194/acp-11-4039-2011.

Akagi, S. K., et al. (2012), Evolution of trace gases and particles emitted by a chaparral fire in California, *Atmos. Chem. Phys.*, *12*(3), 1397–1421, doi:10.5194/acp-12-1397-2012.

Akagi, S. K., et al. (2013), Measurements of reactive trace gases and variable O_3 formation rates in some South Carolina biomass burning plumes, *Atmos. Chem. Phys.*, *13*(3), 1141–1165, doi:10.5194/acp-13-1141-2013.

Alvarado, M. J., and R. G. Prinn (2009), Formation of ozone and growth of aerosols in young smoke plumes from biomass burning: 1. Lagrangian parcel studies, *J. Geophys. Res.*, *114*, D09306, doi:10.1029/2008JD011144.

Alvarado, M. J., C. Wang, and R. G. Prinn (2009), Formation of ozone and growth of aerosols in young smoke plumes from biomass burning: 2. Three-dimensional Eulerian studies, *J. Geophys. Res.*, *114*, D09307, doi:10.1029/2008JD011186.

Alvarado, M. J., et al. (2010), Nitrogen oxides and PAN in plumes from boreal fires during ARCTAS-B and their impact on ozone: An integrated analysis of aircraft and satellite observations, *Atmos. Chem. Phys.*, *10*(20), 9739–9760, doi:10.5194/acp-10-9739-2010.

Andreae, M. O., and P. Merlet (2001), Emission of trace gases and aerosols from biomass burning, *Global Biogeochem. Cycles*, *15*, 955–966, doi:10.1029/2000GB001382.

Atkinson, R., and J. Arey (2003), Atmospheric degradation of volatile organic compounds, *Chem. Rev.*, *103*(12), 4605–4638, doi:10.1021/cr0206420.

Atkinson, R., D. L. Baulch, R. A. Cox, J. N. Crowley, R. F. Hampson, R. G. Hynes, M. E. Jenkin, M. J. Rossi, J. Troe, and I. Subcommittee (2006), Evaluated kinetic and photochemical data for atmospheric chemistry: Volume II-gas phase reactions of organic species, *Atmos. Chem. Phys.*, *6*(11), 3625–4055, doi:10.5194/acp-6-3625-2006.

Bai, J., C. Yu, L. Li, P. Wu, Z. Luo, and M. Ni (2013), Experimental study on the NO and N_2O formation characteristics during biomass combustion, *Energy Fuels*, *27*(1), 515–522, doi:10.1021/ef301383g.

Baylon, P., D. A. Jaffe, N. L. Wigder, H. Gao, and J. Hee (2015), Ozone enhancement in western US wildfire plumes at the Mt. Bachelor Observatory: The role of NO_x, *Atmos. Environ.*, *109*, 297–304, doi:10.1016/j.atmosenv.2014.09.013.

Becidan, M., Ø. Skreiberg, and J. E. Hustad (2007), NO_x and N_2O precursors (NH_3 and HCN) in pyrolysis of biomass residues, *Energy Fuels*, *21*(2), 1173–1180, doi:10.1021/ef060426k.

Bergstrom, R. W., P. B. Russell, and P. Hignett (2002), Wavelength dependence of the absorption of black carbon particles: Predictions and results from the TARFOX experiment and implications for the aerosol single scattering albedo, *J. Atmos. Sci.*, *59*(3), 567–577, doi:10.1175/1520-0469(2002)059<0567:WDOTAO>2.0.CO;2.

Blake, N. J., et al. (2003), NMHCs and halocarbons in Asian continental outflow during the Transport and Chemical Evolution over the Pacific (TRACE-P) field campaign: Comparison with PEM-West B, *J. Geophys. Res.*, *108*(D20), 8806, doi:10.1029/2002JD003367.

Bond, T. C., D. G. Streets, K. F. Yarber, S. M. Nelson, J.-H. Woo, and Z. Klimont (2004), A technology-based global inventory of black and organic carbon emissions from combustion, *J. Geophys. Res.*, *109*, D14203, doi:10.1029/2003JD003697.

Bond, T. C., et al. (2013), Bounding the role of black carbon in the climate system: A scientific assessment, *J. Geophys. Res. Atmos.*, *118*, 5380–5552, doi:10.1002/jgrd.50171.

Burling, I. R., et al. (2010), Laboratory measurements of trace gas emissions from biomass burning of fuel types from the southeastern and southwestern United States, *Atmos. Chem. Phys.*, *10*(22), 11,115–11,130, doi:10.5194/acp-10-11115-2010.

Burling, I. R., R. J. Yokelson, S. K. Akagi, S. P. Urbanski, C. E. Wold, D. W. T. Griffith, T. J. Johnson, J. Reardon, and D. R. Weise (2011), Airborne and ground-based measurements of the trace gases and particles emitted by prescribed fires in the United States, *Atmos. Chem. Phys.*, *11*(23), 12,197–12,216, doi:10.5194/acp-11-12197-2011.

Butkovskaya, N. I., N. Pouvesle, A. Kukui, Y. Mu, and G. Le Bras (2006), Mechanism of the OH-initiated oxidation of hydroxyacetone over the temperature range 236–298 K, *J. Phys. Chem. A*, *110*(21), 6833–6843, doi:10.1021/jp056345r.

Canagaratna, M. R., et al. (2007), Chemical and microphysical characterization of ambient aerosols with the aerodyne aerosol mass spectrometer, *Mass Spectrom. Rev.*, *26*(2), 185–222, doi:10.1002/mas.20115.
Canagaratna, M. R., et al. (2015), Elemental ratio measurements of organic compounds using aerosol mass spectrometry: Characterization, improved calibration, and implications, *Atmos. Chem. Phys.*, *15*(1), 253–272, doi:10.5194/acp-15-253-2015.
Capes, G., B. Johnson, G. McFiggans, P. I. Williams, J. Haywood, and H. Coe (2008), Aging of biomass burning aerosols over West Africa: Aircraft measurements of chemical composition, microphysical properties, and emission ratios, *J. Geophys. Res.*, *113*, D00C15, doi:10.1029/2008JD009845.
Cazorla, M., G. M. Wolfe, S. A. Bailey, A. K. Swanson, H. L. Arkinson, and T. F. Hanisco (2015), A new airborne laser-induced fluorescence instrument for in situ detection of formaldehyde throughout the troposphere and lower stratosphere, *Atmos. Meas. Tech.*, *8*(2), 541–552, doi:10.5194/amt-8-541-2015.
Chan, K. R., J. Dean-Day, S. W. Bowen, and T. P. Bui (1998), Turbulence measurements by the DC-8 meteorological measurement system, *Geophys. Res. Lett.*, *25*, 1355–1358, doi:10.1029/97GL03590.
Chang, D., and Y. Song (2010), Estimates of biomass burning emissions in tropical Asia based on satellite-derived data, *Atmos. Chem. Phys.*, *10*(5), 2335–2351, doi:10.5194/acp-10-2335-2010.
Chen, Y., and T. C. Bond (2010), Light absorption by organic carbon from wood combustion, *Atmos. Chem. Phys.*, *10*(4), 1773–1787, doi:10.5194/acp-10-1773-2010.
Christian, T. J., B. Kleiss, R. J. Yokelson, R. Holzinger, P. J. Crutzen, W. M. Hao, B. H. Saharjo, and D. E. Ward (2003), Comprehensive laboratory measurements of biomass-burning emissions: 1. Emissions from Indonesian, African, and other fuels, *J. Geophys. Res.*, *108*(D23), 4719, doi:10.1029/2003JD003704.
Christian, T. J., R. J. Yokelson, B. Cárdenas, L. T. Molina, G. Engling, and S. C. Hsu (2010), Trace gas and particle emissions from domestic and industrial biofuel use and garbage burning in central Mexico, *Atmos. Chem. Phys.*, *10*(2), 565–584, doi:10.5194/acp-10-565-2010.
Cox, R. A., and J. A. Cole (1985), Chemical aspects of the autoignition of hydrocarbon-air mixtures, *Combust. Flame*, *60*(2), 109–123, doi:10.1016/0010-2180(85)90001-X.
Crounse, J. D., K. A. McKinney, A. J. Kwan, and P. O. Wennberg (2006), Measurement of gas-phase hydroperoxides by chemical ionization mass spectrometry, *Anal. Chem.*, *78*(19), 6726–6732, doi:10.1021/ac0604235.
Crounse, J. D., et al. (2009), Biomass burning and urban air pollution over the Central Mexican Plateau, *Atmos. Chem. Phys.*, *9*(14), 4929–4944, doi:10.5194/acp-9-4929-2009.
Crounse, J. D., F. Paulot, H. G. Kjaergaard, and P. O. Wennberg (2011), Peroxy radical isomerization in the oxidation of isoprene, *Phys. Chem. Chem. Phys.*, *13*(30), 13,607–13,613, doi:10.1039/C1CP21330J.
Crounse, J. D., L. B. Nielsen, S. Jørgensen, H. G. Kjaergaard, and P. O. Wennberg (2013), Autoxidation of organic compounds in the atmosphere, *J. Phys. Chem. Lett.*, *4*(20), 3513–3520, doi:10.1021/jz4019207.
Crutzen, P. J., and M. O. Andreae (1990), Biomass burning in the tropics: Impact on atmospheric chemistry and biogeochemical cycles, *Science*, *250*(4988), 1669–1678, doi:10.1126/science.250.4988.1669.
Cubison, M. J., et al. (2011), Effects of aging on organic aerosol from open biomass burning smoke in aircraft and laboratory studies, *Atmos. Chem. Phys.*, *11*(23), 12,049–12,064, doi:10.5194/acp-11-12049-2011.
Dahneke, B. (1983), Simple kinetic theory of Brownian diffusion in vapors and aerosols, in *Theory of Dispersed Multiphase Flow*, edited by R. E. Meyer, pp. 97–133, Academic, New York.
DeCarlo, P. F., et al. (2008), Fast airborne aerosol size and chemistry measurements above Mexico City and Central Mexico during the MILAGRO campaign, *Atmos. Chem. Phys.*, *8*(14), 4027–4048, doi:10.5194/acp-8-4027-2008.
de Gouw, J. A., C. Warneke, D. D. Parrish, J. S. Holloway, M. Trainer, and F. C. Fehsenfeld (2003), Emission sources and ocean uptake of acetonitrile (CH_3CN) in the atmosphere, *J. Geophys. Res.*, *108*(D11), 4329, doi:10.1029/2002JD002897.
Dennis, A., M. Fraser, S. Anderson, and D. Allen (2002), Air pollutant emissions associated with forest, grassland, and agricultural burning in Texas, *Atmos. Environ.*, *36*(23), 3779–3792, doi:10.1016/S1352-2310(02)00219-4.
Diskin, G. S., J. R. Podolske, G. W. Sachse, and T. A. Slate (2002), Open-path airborne tunable diode laser hygrometer, *Proc. SPIE*, *4817*, 196–204, doi:10.1117/12.453736.
Donahue, N. M., A. L. Robinson, C. O. Stanier, and S. N. Pandis (2006), Coupled partitioning, dilution, and chemical aging of semivolatile organics, *Environ. Sci. Technol.*, *40*(8), 2635–2643, doi:10.1021/es052297c.
Fischer, E. V., et al. (2014), Atmospheric peroxyacetyl nitrate (PAN): A global budget and source attribution, *Atmos. Chem. Phys.*, *14*(5), 2679–2698, doi:10.5194/acp-14-2679-2014.
Forrister, H., et al. (2015), Evolution of brown carbon in wildfire plumes, *Geophys. Res. Lett.*, *42*, 4623–4630, doi:10.1002/2015GL063897.
Goode, J. G., R. J. Yokelson, D. E. Ward, R. A. Susott, R. E. Babbitt, M. A. Davies, and W. M. Hao (2000), Measurements of excess O_3, CO_2, CO, CH_4, C_2H_4, C_2H_2, HCN, NO, NH_3, HCOOH, CH_3COOH, HCHO, and CH_3OH in 1997 Alaskan biomass burning plumes by airborne Fourier transform infrared spectroscopy (AFTIR), *J. Geophys. Res.*, *105*, 22,147–22,166, doi:10.1029/2000JD900287.
Gray, B. A., Y. Wang, D. Gu, A. Bandy, L. Mauldin, A. Clarke, B. Alexander, and D. D. Davis (2010), Sources, transport, and sinks of SO_2 over the equatorial Pacific during the Pacific atmospheric sulfur experiment, *J. Atmos. Chem.*, *68*(1), 27–53, doi:10.1007/s10874-010-9177-7.
Grieshop, A. P., N. M. Donahue, and A. L. Robinson (2009), Laboratory investigation of photochemical oxidation of organic aerosol from wood fires 2: Analysis of aerosol mass spectrometer data, *Atmos. Chem. Phys.*, *9*(6), 2227–2240, doi:10.5194/acp-9-2227-2009.
Grosjean, D., E. L. Williams, and E. Grosjean (1993), Atmospheric chemistry of isoprene and of its carbonyl products, *Environ. Sci. Technol.*, *27*(5), 830–840, doi:10.1021/es00042a004.
Hawbaker, T. J., V. C. Radeloff, A. D. Syphard, Z. Zhu, and S. I. Stewart (2008), Detection rates of the MODIS active fire product in the United States, *Remote Sens. Environ.*, *112*(5), 2656–2664, doi:10.1016/j.rse.2007.12.008.
Hayashi, K., K. Ono, M. Kajiura, S. Sudo, S. Yonemura, A. Fushimi, K. Saitoh, Y. Fujitani, and K. Tanabe (2014), Trace gas and particle emissions from open burning of three cereal crop residues: Increase in residue moistness enhances emissions of carbon monoxide, methane, and particulate organic carbon, *Atmos. Environ.*, *95*, 36–44, doi:10.1016/j.atmosenv.2014.06.023.
Hayes, P. L., et al. (2015), Modeling the formation and aging of secondary organic aerosols in Los Angeles during CalNex 2010, *Atmos. Chem. Phys.*, *15*(10), 5773–5801, doi:10.5194/acp-15-5773-2015.
Hecobian, A., et al. (2011), Comparison of chemical characteristics of 495 biomass burning plumes intercepted by the NASA DC-8 aircraft during the ARCTAS/CARB-2008 field campaign, *Atmos. Chem. Phys.*, *11*(24), 13,325–13,337, doi:10.5194/acp-11-13325-2011.
Hennigan, C. J., et al. (2011), Chemical and physical transformations of organic aerosol from the photo-oxidation of open biomass burning emissions in an environmental chamber, *Atmos. Chem. Phys.*, *11*(15), 7669–7686, doi:10.5194/acp-11-7669-2011.
Hobbs, P. V., P. Sinha, R. J. Yokelson, T. J. Christian, D. R. Blake, S. Gao, T. W. Kirchstetter, T. Novakov, and P. Pilewskie (2003), Evolution of gases and particles from a savanna fire in South Africa, *J. Geophys. Res.*, *108*(D13), 8485, doi:10.1029/2002JD002352.

Hodzic, A., and J. L. Jimenez (2011), Modeling anthropogenically controlled secondary organic aerosols in a megacity: A simplified framework for global and climate models, *Geosci. Model Dev.*, *4*(4), 901–917, doi:10.5194/gmd-4-901-2011.

Hosseini, S., et al. (2013), Laboratory characterization of PM emissions from combustion of wildland biomass fuels, *J. Geophys. Res. Atmos.*, *118*, 9914–9929, doi:10.1002/jgrd.50481.

Huang, X., M. Li, J. Li, and Y. Song (2012), A high-resolution emission inventory of crop burning in fields in China based on MODIS thermal anomalies/fire products, *Atmos. Environ.*, *50*, 9–15, doi:10.1016/j.atmosenv.2012.01.017.

Huey, L. G., et al. (2004), CIMS measurements of HNO_3 and SO_2 at the South Pole during ISCAT 2000, *Atmos. Environ.*, *38*(32), 5411–5421, doi:10.1016/j.atmosenv.2004.04.037.

Jacob, D. J., et al. (1992), Summertime photochemistry of the troposphere at high northern latitudes, *J. Geophys. Res.*, *97*, 16,421–16,431, doi:10.1029/91JD01968.

Jaffe, D. A., and N. L. Wigder (2012), Ozone production from wildfires: A critical review, *Atmos. Environ.*, *51*, 1–10, doi:10.1016/j.atmosenv.2011.11.063.

Jolleys, M. D., et al. (2012), Characterizing the aging of biomass burning organic aerosol by use of mixing ratios: A meta-analysis of four regions, *Environ. Sci. Technol.*, *46*(24), 13,093–13,102, doi:10.1021/es302386v.

Jolleys, M. D., H. Coe, G. McFiggans, G. R. McMeeking, T. Lee, S. M. Kreidenweis, J. L. Collett, and A. P. Sullivan (2014), Organic aerosol emission ratios from the laboratory combustion of biomass fuels, *J. Geophys. Res. Atmos.*, *119*, 12,850–12,871, doi:10.1002/2014JD021589.

Jost, C., J. Trentmann, D. Sprung, M. O. Andreae, J. B. McQuaid, and H. Barjat (2003), Trace gas chemistry in a young biomass burning plume over Namibia: Observations and model simulations, *J. Geophys. Res.*, *108*(D13), 8482, doi:10.1029/2002JD002431.

Kirchstetter, T. W., T. Novakov, and P. V. Hobbs (2004), Evidence that the spectral dependence of light absorption by aerosols is affected by organic carbon, *J. Geophys. Res.*, *109*, D21208, doi:10.1029/2004JD004999.

Kondo, Y., et al. (2004), Impacts of biomass burning in Southeast Asia on ozone and reactive nitrogen over the western Pacific in spring, *J. Geophys. Res.*, *109*, D15S12, doi:10.1029/2003JD004203.

Kudo, S., et al. (2014), Emissions of nonmethane volatile organic compounds from open crop residue burning in the Yangtze River Delta region, China, *J. Geophys. Res. Atmos.*, *119*, 7684–7698, doi:10.1002/2013JD021044.

Lack, D. A., and J. M. Langridge (2013), On the attribution of black and brown carbon light absorption using the Ångström exponent, *Atmos. Chem. Phys.*, *13*(20), 10,535–10,543, doi:10.5194/acp-13-10535-2013.

Lack, D. A., J. M. Langridge, R. Bahreini, C. D. Cappa, A. M. Middlebrook, and J. P. Schwarz (2012), Brown carbon and internal mixing in biomass burning particles, *Proc. Natl. Acad. Sci. U. S. A.*, *109*(37), 14,802–14,807.

Lee, H. J., P. K. Aiona, A. Laskin, J. Laskin, and S. A. Nizkorodov (2014), Effect of solar radiation on the optical properties and molecular composition of laboratory proxies of atmospheric brown carbon, *Environ. Sci. Technol.*, *48*(17), 10,217–10,226, doi:10.1021/es502515r.

Lee, M., B. G. Heikes, and D. J. Jacob (1998), Enhancements of hydroperoxides and formaldehyde in biomass burning impacted air and their effect on atmospheric oxidant cycles, *J. Geophys. Res.*, *103*, 13,201–13,212, doi:10.1029/98JD00578.

Leung, F.-Y. T., J. A. Logan, R. Park, E. Hyer, E. Kasischke, D. Streets, and L. Yurganov (2007), Impacts of enhanced biomass burning in the boreal forests in 1998 on tropospheric chemistry and the sensitivity of model results to the injection height of emissions, *J. Geophys. Res.*, *112*, D10313, doi:10.1029/2006JD008132.

Li, Q., D. J. Jacob, I. Bey, R. M. Yantosca, Y. Zhao, Y. Kondo, and J. Notholt (2000), Atmospheric hydrogen cyanide (HCN): Biomass burning source, ocean sink?, *Geophys. Res. Lett.*, *27*, 357–360, doi:10.1029/1999GL010935.

Li, Q., D. J. Jacob, R. M. Yantosca, C. L. Heald, H. B. Singh, M. Koike, Y. Zhao, G. W. Sachse, and D. G. Streets (2003), A global three-dimensional model analysis of the atmospheric budgets of HCN and CH_3CN: Constraints from aircraft and ground measurements, *J. Geophys. Res.*, *108*(D21), 8827, doi:10.1029/2002JD003075.

Lin, X., M. Trainer, and S. C. Liu (1988), On the nonlinearity of the tropospheric ozone production, *J. Geophys. Res.*, *93*, 15,879–15,888, doi:10.1029/JD093iD12p15879.

Liu, J., M. Bergin, H. Guo, L. King, N. Kotra, E. Edgerton, and R. J. Weber (2013), Size-resolved measurements of brown carbon in water and methanol extracts and estimates of their contribution to ambient fine-particle light absorption, *Atmos. Chem. Phys.*, *13*(24), 12,389–12,404, doi:10.5194/acp-13-12389-2013.

Liu, J., et al. (2014), Brown carbon in the continental troposphere, *Geophys. Res. Lett.*, *41*, 2191–2195, doi:10.1002/2013GL058976.

Liu, J., et al. (2015), Brown carbon aerosol in the North American continental troposphere: Sources, abundance, and radiative forcing, *Atmos. Chem. Phys.*, *15*(14), 7841–7858, doi:10.5194/acp-15-7841-2015.

Liu, S. C., M. Trainer, F. C. Fehsenfeld, D. D. Parrish, E. J. Williams, D. W. Fahey, G. Hübler, and P. C. Murphy (1987), Ozone production in the rural troposphere and the implications for regional and global ozone distributions, *J. Geophys. Res.*, *92*, 4191–4207, doi:10.1029/JD092iD04p04191.

Liu, Z., et al. (2010), Evidence of reactive aromatics as a major source of peroxy acetyl nitrate over China, *Environ. Sci. Technol.*, *44*(18), 7017–7022, doi:10.1021/es1007966.

Liu, Z., et al. (2012), Summertime photochemistry during CAREBeijing-2007: RO_x budgets and O_3 formation, *Atmos. Chem. Phys.*, *12*(16), 7737–7752, doi:10.5194/acp-12-7737-2012.

Lobert, J. M., D. H. Scharffe, W. M. Hao, T. A. Kuhlbusch, R. Seuwen, P. Warneck, and P. J. Crutzen (1991), Experimental evaluation of biomass burning emissions: Nitrogen and carbon containing compounds, in *Global Biomass Burning: Atmospheric, Climatic, and Biospheric Implications*, edited by J. S. Levine, pp. 289–304 , MIT Press, Cambridge, Mass.

Marion, T., P. E. Perros, R. Losno, and E. Steiner (2001), Ozone production efficiency in savanna and forested areas during the EXPRESSO experiment, *J. Atmos. Chem.*, *38*(1), 3–30, doi:10.1023/A:1026585603100.

Mason, S. A., R. J. Field, R. J. Yokelson, M. A. Kochivar, M. R. Tinsley, D. E. Ward, and W. M. Hao (2001), Complex effects arising in smoke plume simulations due to inclusion of direct emissions of oxygenated organic species from biomass combustion, *J. Geophys. Res.*, *106*, 12,527–12,539, doi:10.1029/2001JD900003.

Mason, S. A., J. Trentmann, T. Winterrath, R. J. Yokelson, T. J. Christian, L. J. Carlson, T. R. Warner, L. C. Wolfe, and M. O. Andreae (2006), Intercomparison of two box models of the chemical evolution in biomass-burning smoke plumes, *J. Atmos. Chem.*, *55*(3), 273–297, doi:10.1007/s10874-006-9039-5.

May, A. A., E. J. T. Levin, C. J. Hennigan, I. Riipinen, T. Lee, J. L. Collett, J. L. Jimenez, S. M. Kreidenweis, and A. L. Robinson (2013), Gas-particle partitioning of primary organic aerosol emissions: 3. Biomass burning, *J. Geophys. Res. Atmos.*, *118*, 11,327–11,338, doi:10.1002/jgrd.50828.

McCarty, J. L. (2011), Remote sensing-based estimates of annual and seasonal emissions from crop residue burning in the contiguous United States, *J. Air Waste Manage. Assoc.*, *61*(1), 22–34, doi:10.3155/1047-3289.61.1.22.

McCarty, J. L., C. Justice, and S. Korontzi (2007), Agricultural burning in the southeastern United States detected by MODIS, *Remote Sens. Environ.*, *108*(2), 151–162, doi:10.1016/j.rse.2006.03.020.

McCarty, J. L., S. Korontzi, C. O. Justice, and T. Loboda (2009), The spatial and temporal distribution of crop residue burning in the contiguous United States, *Sci. Total Environ.*, *407*(21), 5701–5712, doi:10.1016/j.scitotenv.2009.07.009.

McMeeking, G. R., et al. (2009), Emissions of trace gases and aerosols during the open combustion of biomass in the laboratory, *J. Geophys. Res.*, *114*, D19210, doi:10.1029/2009JD011836.

Melvin, M. A. (2012), 2012 national prescribed fire use survey report, *Tech. Rep. 01-12*, Coalition of Prescribed Fire Counc., Inc.

Millet, D. B., et al. (2010), Global atmospheric budget of acetaldehyde: 3-D model analysis and constraints from in-situ and satellite observations, *Atmos. Chem. Phys.*, *10*(7), 3405–3425, doi:10.5194/acp-10-3405-2010.

Müller, M., et al. (2016), In situ measurements and modeling of reactive trace gases in a small biomass burning plume, *Atmos. Chem. Phys.*, *16*(6), 3813–3824, doi:10.5194/acp-16-3813-2016.

Oanh, N. T. K., T. L. Bich, D. Tipayarom, B. R. Manadhar, P. Prapat, C. D. Simpson, and L. J. S. Liu (2011), Characterization of particulate matter emission from open burning of rice straw, *Atmos. Environ.*, *45*(2), 493–502, doi:10.1016/j.atmosenv.2010.09.023.

Olszyna, K. J., E. M. Bailey, R. Simonaitis, and J. F. Meagher (1994), O_3 and NO_y relationships at a rural site, *J. Geophys. Res.*, *99*, 14,557–14,563, doi:10.1029/94JD00739.

Orlando, J. J., and G. S. Tyndall (2012), Laboratory studies of organic peroxy radical chemistry: An overview with emphasis on recent issues of atmospheric significance, *Chem. Soc. Rev.*, *41*(19), 6294–6317, doi:10.1039/C2CS35166H.

Ortega, A. M., D. A. Day, M. J. Cubison, W. H. Brune, D. Bon, J. A. de Gouw, and J. L. Jimenez (2013), Secondary organic aerosol formation and primary organic aerosol oxidation from biomass-burning smoke in a flow reactor during FLAME-3, *Atmos. Chem. Phys.*, *13*(22), 11,551–11,571, doi:10.5194/acp-13-11551-2013.

Paulot, F., J. D. Crounse, H. G. Kjaergaard, J. H. Kroll, J. H. Seinfeld, and P. O. Wennberg (2009a), Isoprene photooxidation: New insights into the production of acids and organic nitrates, *Atmos. Chem. Phys.*, *9*(4), 1479–1501, doi:10.5194/acp-9-1479-2009.

Paulot, F., J. D. Crounse, H. G. Kjaergaard, A. Kurten, J. M. S. Clair, J. H. Seinfeld, and P. O. Wennberg (2009b), Unexpected epoxide formation in the gas-phase photooxidation of isoprene, *Science*, *325*(5941), 730–733, doi:10.1126/science.1172910.

Randerson, J. T., Y. Chen, G. R. van der Werf, B. M. Rogers, and D. C. Morton (2012), Global burned area and biomass burning emissions from small fires, *J. Geophys. Res.*, *117*, G04012, doi:10.1029/2012JG002128.

Reid, J. S., R. Koppmann, T. F. Eck, and D. P. Eleuterio (2005), A review of biomass burning emissions part II: Intensive physical properties of biomass burning particles, *Atmos. Chem. Phys.*, *5*(3), 799–825, doi:10.5194/acp-5-799-2005.

Reid, S. B., T. H. Funk, D. C. Sullivan, P. S. Stiefer, H. L. Arkinson, S. G. Brown, and L. R. Chinkin (2004), Research and development of emission inventories for planned burning activities for the Central State Regional Air Planning Association, paper presented at 13th International Emission Inventory Conference, Clearwater, Fla., June 8–10.

Rogge, W. F., L. M. Hildemann, M. A. Mazurek, G. R. Cass, and B. R. T. Simoneit (1991), Sources of fine organic aerosol. 1. Charbroilers and meat cooking operations, *Environ. Sci. Technol.*, *25*(6), 1112–1125, doi:10.1021/es00018a015.

Ryerson, T. B., L. G. Huey, K. Knapp, J. A. Neuman, D. D. Parrish, D. T. Sueper, and F. C. Fehsenfeld (1999), Design and initial characterization of an inlet for gas-phase NO_y measurements from aircraft, *J. Geophys. Res.*, *104*, 5483–5492, doi:10.1029/1998JD100087.

Ryerson, T. B., E. J. Williams, and F. C. Fehsenfeld (2000), An efficient photolysis system for fast-response NO_2 measurements, *J. Geophys. Res.*, *105*, 26,447–26,461, doi:10.1029/2000JD900389.

Sachse, G. W., G. F. Hill, L. O. Wade, and M. G. Perry (1987), Fast-response, high-precision carbon monoxide sensor using a tunable diode laser absorption technique, *J. Geophys. Res.*, *92*, 2071–2081, doi:10.1029/JD092iD02p02071.

Saleh, R., C. J. Hennigan, G. R. McMeeking, W. K. Chuang, E. S. Robinson, H. Coe, N. M. Donahue, and A. L. Robinson (2013), Absorptivity of brown carbon in fresh and photo-chemically aged biomass-burning emissions, *Atmos. Chem. Phys.*, *13*(15), 7683–7693, doi:10.5194/acp-13-7683-2013.

Sander, S. P., et al. (2011), *Chemical Kinetics and Photochemical Data for Use in Atmospheric Studies, Evaluation No. 17*, *JPL Publ. 10-6*, Jet Propul. Lab., Pasadena, Calif.

Schnaiter, M., et al. (2005), Measurement of wavelength-resolved light absorption by aerosols utilizing a UV-VIS extinction cell, *Aerosol Sci. Technol.*, *39*(3), 249–260, doi:10.1080/027868290925958.

Schwarz, J. P., B. H. Samset, A. E. Perring, J. R. Spackman, R. S. Gao, P. Stier, M. Schulz, F. L. Moore, E. A. Ray, and D. W. Fahey (2013), Global-scale seasonally resolved black carbon vertical profiles over the Pacific, *Geophys. Res. Lett.*, *40*, 5542–5547, doi:10.1002/2013GL057775.

Seiler, W., and P. Crutzen (1980), Estimates of gross and net fluxes of carbon between the biosphere and the atmosphere from biomass burning, *Clim. Change*, *2*(3), 207–247, doi:10.1007/BF00137988.

Shetter, R. E., and M. Müller (1999), Photolysis frequency measurements using actinic flux spectroradiometry during the PEM-Tropics mission: Instrumentation description and some results, *J. Geophys. Res.*, *104*, 5647–5661, doi:10.1029/98JD01381.

Shirai, T., et al. (2003), Emission estimates of selected volatile organic compounds from tropical savanna burning in northern Australia, *J. Geophys. Res.*, *108*(D3), 8406, doi:10.1029/2001JD000841.

Simpson, I. J., et al. (2011), Boreal forest fire emissions in fresh Canadian smoke plumes: C_1-C_{10} volatile organic compounds (VOCs), CO_2, CO, NO_2, NO, HCN and CH_3CN, *Atmos. Chem. Phys.*, *11*(13), 6445–6463, doi:10.5194/acp-11-6445-2011.

Singh, H. B., M. Kanakidou, P. J. Crutzen, and D. J. Jacob (1995), High concentrations and photochemical fate of oxygenated hydrocarbons in the global troposphere, *Nature*, *378*(6552), 50–54.

Singh, H. B., et al. (2010), Pollution influences on atmospheric composition and chemistry at high northern latitudes: Boreal and California forest fire emissions, *Atmos. Environ.*, *44*(36), 4553–4564, doi:10.1016/j.atmosenv.2010.08.026.

Slusher, D. L., L. G. Huey, D. J. Tanner, F. M. Flocke, and J. M. Roberts (2004), A thermal dissociation-chemical ionization mass spectrometry (TD-CIMS) technique for the simultaneous measurement of peroxyacyl nitrates and dinitrogen pentoxide, *J. Geophys. Res.*, *109*, D19315, doi:10.1029/2004JD004670.

Smith, R., M. Adams, S. Maier, R. Craig, A. Kristina, and I. Maling (2007), Estimating the area of stubble burning from the number of active fires detected by satellite, *Remote Sens. Environ.*, *109*(1), 95–106, doi:10.1016/j.rse.2006.12.011.

St. Clair, J. M., K. M. Spencer, M. R. Beaver, J. D. Crounse, F. Paulot, and P. O. Wennberg (2014), Quantification of hydroxyacetone and glycolaldehyde using chemical ionization mass spectrometry, *Atmos. Chem. Phys.*, *14*(8), 4251–4262, doi:10.5194/acp-14-4251-2014.

Stockwell, C. E., R. J. Yokelson, S. M. Kreidenweis, A. L. Robinson, P. J. DeMott, R. C. Sullivan, J. Reardon, K. C. Ryan, D. W. T. Griffith, and L. Stevens (2014), Trace gas emissions from combustion of peat, crop residue, domestic biofuels, grasses, and other fuels: Configuration and Fourier transform infrared (FTIR) component of the fourth Fire Lab at Missoula Experiment (FLAME-4), *Atmos. Chem. Phys.*, *14*(18), 9727–9754, doi:10.5194/acp-14-9727-2014.

Stockwell, C. E., P. R. Veres, J. Williams, and R. J. Yokelson (2015), Characterization of biomass burning emissions from cooking fires, peat, crop residue, and other fuels with high-resolution proton-transfer-reaction time-of-flight mass spectrometry, *Atmos. Chem. Phys.*, *15*(2), 845–865, doi:10.5194/acp-15-845-2015.

Takegawa, N., et al. (2003), Photochemical production of O_3 in biomass burning plumes in the boundary layer over northern Australia, *Geophys. Res. Lett.*, *30*(10), 1500, doi:10.1029/2003GL017017.
Toon, O. B., et al. (2016), Planning, implementation and scientific goals of the Studies of Emissions and Atmospheric Composition, Clouds and Climate Coupling by Regional Surveys (SEAC^{4}RS) field mission, *J. Geophys. Res. Atmos.*, *121*, 4967–5009, doi:10.1002/2015JD024297.
Trainer, M., et al. (1993), Correlation of ozone with NO_y in photochemically aged air, *J. Geophys. Res.*, *98*, 2917–2925, doi:10.1029/92JD01910.
Trentmann, J., and M. O. Andreae (2003), Chemical processes in a young biomass-burning plume, *J. Geophys. Res.*, *108*(D22), 4705, doi:10.1029/2003JD003732.
Trentmann, J., B. Früh, O. Boucher, T. Trautmann, and M. O. Andreae (2003), Three-dimensional solar radiation effects on the actinic flux field in a biomass-burning plume, *J. Geophys. Res.*, *108*(D17), 4558, doi:10.1029/2003JD003422.
Trentmann, J., R. J. Yokelson, P. V. Hobbs, T. Winterrath, T. J. Christian, M. O. Andreae, and S. A. Mason (2005), An analysis of the chemical processes in the smoke plume from a savanna fire, *J. Geophys. Res.*, *110*, D12301, doi:10.1029/2004JD005628.
Tsujimoto, Y., Y. Yamamoto, K. Hayashi, A. I. Zakaria, Y. Inusah, T. Hatta, M. Fosu, and J.-I. Sakagami (2013), Topographic distribution of the soil total carbon content and sulfur deficiency for rice cultivation in a floodplain ecosystem of the northern region of Ghana, *Field Crops Res.*, *152*, 74–82, doi:10.1016/j.fcr.2012.11.007.
Vakkari, V., et al. (2014), Rapid changes in biomass burning aerosols by atmospheric oxidation, *Geophys. Res. Lett.*, *41*, 2644–2651, doi:10.1002/2014GL059396.
van der Werf, G. R., J. T. Randerson, L. Giglio, G. J. Collatz, M. Mu, P. S. Kasibhatla, D. C. Morton, R. S. DeFries, Y. Jin, and T. T. van Leeuwen (2010), Global fire emissions and the contribution of deforestation, savanna, forest, agricultural, and peat fires (1997–2009), *Atmos. Chem. Phys.*, *10*(23), 11,707–11,735, doi:10.5194/acp-10-11707-2010.
Vay, S. A., et al. (2011), Patterns of CO_2 and radiocarbon across high northern latitudes during International Polar Year 2008, *J. Geophys. Res.*, *116*, D14301, doi:10.1029/2011JD015643.
Virkkula, A. (2010), Correction of the calibration of the 3-wavelength Particle Soot Absorption Photometer (3λ PSAP), *Aerosol Sci. Technol.*, *44*(8), 706–712, doi:10.1080/02786826.2010.482110.
Virkkula, A., N. C. Ahlquist, D. S. Covert, W. P. Arnott, P. J. Sheridan, P. K. Quinn, and D. J. Coffman (2005), Modification, calibration and a field test of an instrument for measuring light absorption by particles, *Aerosol Sci. Technol.*, *39*(1), 68–83, doi:10.1080/027868290901963.
Wang, Y., Y. Choi, T. Zeng, D. Davis, M. Buhr, L. Gregory Huey, and W. Neff (2007), Assessing the photochemical impact of snow NO_x emissions over Antarctica during ANTCI 2003, *Atmos. Environ.*, *41*(19), 3944–3958, doi:10.1016/j.atmosenv.2007.01.056.
Washenfelder, R. A., et al. (2015), Biomass burning dominates brown carbon absorption in the rural southeastern United States, *Geophys. Res. Lett.*, *42*, 653–664, doi:10.1002/2014GL062444.
Weibring, P., D. Richter, A. Fried, J. G. Walega, and C. Dyroff (2006), Ultra-high-precision mid-IR spectrometer II: System description and spectroscopic performance, *Appl. Phys. B*, *85*(2-3), 207–218, doi:10.1007/s00340-006-2300-4.
Weibring, P., D. Richter, J. G. Walega, and A. Fried (2007), First demonstration of a high performance difference frequency spectrometer on airborne platforms, *Opt. Express*, *15*(21), 13,476–13,495, doi:10.1364/OE.15.013476.
Wilhelm Scherer, H. (2009), Sulfur in soils, *J. Plant Nutr. Soil Sci.*, *172*(3), 326–335, doi:10.1002/jpln.200900037.
Wisthaler, A., A. Hansel, R. R. Dickerson, and P. J. Crutzen (2002), Organic trace gas measurements by PTR-MS during INDOEX 1999, *J. Geophys. Res.*, *107*(D19), 8024, doi:10.1029/2001JD000576.
Xiong, F., et al. (2015), Observation of isoprene hydroxynitrates in the southeastern United States and implications for the fate of NO_x, *Atmos. Chem. Phys.*, *15*(19), 11,257–11,272, doi:10.5194/acp-15-11257-2015.
Yevich, R., and J. A. Logan (2003), An assessment of biofuel use and burning of agricultural waste in the developing world, *Global Biogeochem. Cycles*, *17*(4), 1095, doi:10.1029/2002GB001952.
Yokelson, R. J., D. W. T. Griffith, and D. E. Ward (1996), Open-path Fourier transform infrared studies of large-scale laboratory biomass fires, *J. Geophys. Res.*, *101*, 21,067–21,080, doi:10.1029/96JD01800.
Yokelson, R. J., J. G. Goode, D. E. Ward, R. A. Susott, R. E. Babbitt, D. D. Wade, I. Bertschi, D. W. T. Griffith, and W. M. Hao (1999), Emissions of formaldehyde, acetic acid, methanol, and other trace gases from biomass fires in North Carolina measured by airborne Fourier transform infrared spectroscopy, *J. Geophys. Res.*, *104*, 30,109–30,125, doi:10.1029/1999JD900817.
Yokelson, R. J., I. T. Bertschi, T. J. Christian, P. V. Hobbs, D. E. Ward, and W. M. Hao (2003), Trace gas measurements in nascent, aged, and cloud-processed smoke from African savanna fires by airborne Fourier transform infrared spectroscopy (AFTIR), *J. Geophys. Res.*, *108*(D13), 8478, doi:10.1029/2002JD002322.
Yokelson, R. J., T. Karl, P. Artaxo, D. R. Blake, T. J. Christian, D. W. T. Griffith, A. Guenther, and W. M. Hao (2007), The tropical forest and fire emissions experiment: Overview and airborne fire emission factor measurements, *Atmos. Chem. Phys.*, *7*(19), 5175–5196, doi:10.5194/acp-7-5175-2007.
Yokelson, R. J., T. J. Christian, T. G. Karl, and A. Guenther (2008), The tropical forest and fire emissions experiment: Laboratory fire measurements and synthesis of campaign data, *Atmos. Chem. Phys.*, *8*(13), 3509–3527, doi:10.5194/acp-8-3509-2008.
Yokelson, R. J., et al. (2009), Emissions from biomass burning in the Yucatan, *Atmos. Chem. Phys.*, *9*(15), 5785–5812, doi:10.5194/acp-9-5785-2009.
Yokelson, R. J., I. R. Burling, S. P. Urbanski, E. L. Atlas, K. Adachi, P. R. Buseck, C. Wiedinmyer, S. K. Akagi, D. W. Toohey, and C. E. Wold (2011), Trace gas and particle emissions from open biomass burning in Mexico, *Atmos. Chem. Phys.*, *11*(14), 6787–6808, doi:10.5194/acp-11-6787-2011.
Yokelson, R. J., et al. (2013), Coupling field and laboratory measurements to estimate the emission factors of identified and unidentified trace gases for prescribed fires, *Atmos. Chem. Phys.*, *13*(1), 89–116, doi:10.5194/acp-13-89-2013.
Zhang, L., R. Vet, J. M. O'Brien, C. Mihele, Z. Liang, and A. Wiebe (2009), Dry deposition of individual nitrogen species at eight Canadian rural sites, *J. Geophys. Res.*, *114*, D02301, doi:10.1029/2008JD010640.
Zhang, Y., Y. Wang, B. A. Gray, D. Gu, L. Mauldin, C. Cantrell, and A. Bandy (2014), Surface and free tropospheric sources of methanesulfonic acid over the tropical Pacific Ocean, *Geophys. Res. Lett.*, *41*, 5239–5245, doi:10.1002/2014GL060934.
Zhang, Y., et al. (2016), Large vertical gradient of reactive nitrogen oxides in the boundary layer: Modeling analysis of DISCOVER-AQ 2011 observations, *J. Geophys. Res. Atmos.*, *121*, 1922–1934, doi:10.1002/2015JD024203.
Zhang, Y. L., et al. (2015), Fossil vs. non-fossil sources of fine carbonaceous aerosols in four Chinese cities during the extreme winter haze episode of 2013, *Atmos. Chem. Phys.*, *15*(3), 1299–1312, doi:10.5194/acp-15-1299-2015.
Zhao, R., A. K. Y. Lee, L. Huang, X. Li, F. Yang, and J. P. D. Abbatt (2015), Photochemical processing of aqueous atmospheric brown carbon, *Atmos. Chem. Phys.*, *15*(11), 6087–6100, doi:10.5194/acp-15-6087-2015.
Zhong, M., and M. Jang (2014), Dynamic light absorption of biomass-burning organic carbon photochemically aged under natural sunlight, *Atmos. Chem. Phys.*, *14*(3), 1517–1525, doi:10.5194/acp-14-1517-2014.